

1 Molecular mechanisms underlying attenuation of live attenuated Japanese encephalitis virus  
2 vaccine SA14-14-2.

3 Pooja Hoovina Venkatesh<sup>1§</sup>, Saurabh Kumar<sup>1§</sup>, Naveen Kumar<sup>1§</sup>, Krishna Chaitanya<sup>1</sup>, Lance  
4 Turtle<sup>2</sup>, Vijaya Satchidanandam<sup>1,\*</sup>

5

6 <sup>1</sup>Department of Microbiology and Cell Biology, Indian Institute of Science, Bangalore 560012,  
7 INDIA.

8 <sup>2</sup>NIHR Health Protection Research Unit for Emerging and Zoonotic Infections, Institute of  
9 Infection, Veterinary and Ecological Sciences, University of Liverpool, 8 West Derby Street,  
10 Liverpool, L69 7BE, UK and Tropical & Infectious Disease Unit, Royal Liverpool University  
11 Hospital, Liverpool, L7 8XP, UK.

12

13 § These authors contributed equally to this study.

14

15 \*Correspondence author: Vijaya Satchidanandam; Email: [vijaya@iisc.ac.in](mailto:vijaya@iisc.ac.in)

16 **Short Title:** Mode of attenuation of SA14-14-2

17 **ABSTRACT**

18 The live attenuated Japanese encephalitis virus vaccine SA14-14-2 demonstrated  $\geq 95\%$   
19 efficacy and is today the vaccine of choice against JEV globally. Relative to its parent strain  
20 SA14, SA14-14-2 carries 46 nucleotide and 24 amino acid alterations, with 8 of the latter  
21 located within the envelope glycoprotein. The vaccine strain also fails to synthesize the  
22 nonstructural protein NS1' owing to a silent mutation that abrogates a -1-frameshifting event  
23 close to the 5' end of the NS2A coding sequence. Previous studies employing reverse genetics  
24 and mouse models implicated both absence of NS1' and mutated E, in attenuation of SA14-  
25 14-2. We demonstrate progressive reduction in ER stress sensor PERK levels and increased  
26 expression of CEBP-homologous protein (CHOP), accompanied by dephosphorylation of  
27 eIF2 $\alpha$ , inhibition of autophagy maturation and necroptosis following infection of cultured cells  
28 with wild-type JEV strain P20778. Autonomous expression of NS1' caused constitutive up-  
29 regulation of CHOP and loss of PERK. Conversely, infection with SA14-14-2 led to  
30 significantly increased IRE-1 $\alpha$  activation, ER chaperone levels and autophagy. We report labile  
31 conformational epitopes accompanied by drastically reduced folding kinetics of intracellular  
32 SA14-14-2 envelope protein engendered by sluggish oxidation of cysteine sulfhydryl groups  
33 to form disulfide bonds within the endoplasmic reticulum along with altered envelope epitopes  
34 in extracellular SA14-14-2 viral particles. We also demonstrate near total conversion of prM  
35 to pr and M in SA14-14-2 virus particles. These alterations were accompanied by enhanced  
36 activation of mouse and human antigen presenting cells by SA14-14-2 along with superior  
37 CD8<sup>+</sup> recall T cell responses to viral structural proteins in volunteers vaccinated with SA14-  
38 14-2.

39 **Author Summary:** The random process of cell culture passage adopted in generation of most  
40 live attenuated virus vaccines leads to fixation of multiple nucleotide changes in their genomes  
41 and renders it difficult if not impossible to pinpoint those mutations primarily responsible for

42 their attenuated phenotype. Identifying the precise attenuating mutations and their *modi*  
43 *operandi* should aid in developing rationally attenuated vaccines for other viruses. We  
44 discovered that wild type (WT) JEV uses the nonstructural protein NS1' to take over the host  
45 protein synthesis machinery to produce viral proteins. Loss of NS1' in SA14-14-2 deprives the  
46 vaccine strain of this ability. Viruses uniformly target host death pathways to avoid generating  
47 potent antiviral immune responses. WT JEV prevents autophagy maturation. Conversely the  
48 SA14-14-2 vaccine activates autophagy due to unresolved ER stress caused by inability of its  
49 envelope glycoprotein to fold promptly post synthesis. Combined with enhanced proteolytic  
50 cleavage of the viral prM protein in SA14-14-2, this resulted in altered envelope epitopes on  
51 extracellular SA14-14-2 virus particles. These changes culminated in enhanced activation of  
52 innate and adaptive immune responses by SA14-14-2.

## 53 INTRODUCTION

54 The genus *Flavivirus*, in the family Flaviviridae, comprising numerous vector-borne human  
55 pathogens has spawned two highly efficacious live attenuated vaccines in Yellow Fever virus  
56 (YFV)-17D and Japanese encephalitis virus (JEV) -SA14-14-2, both of which have contributed  
57 to significant reduction of disease incidence from their respective viral pathogens. Flavivirus  
58 genomes are single strand RNA of positive polarity and encode a single large polyprotein  
59 which is processed by host and virally encoded proteases to give rise to 3 structural (capsid, C;  
60 envelope, E; and premembrane, prM) and 7 non-structural (NS; 1, 2A, 2B, 3, 4A, 4B and 5)  
61 proteins. JEV is represented by a single serotype and 5 genotypes [1] and was first isolated in  
62 Japan in 1934, giving us the prototype Nakayama strain [2]. Based on meta-analysis of  
63 published literature and national incidence estimates of 124 countries the annual global  
64 incidence of JEV encephalitis was computed around 67,900 [3].

65 Of the 24 amino acid changes identified in SA14-14-2 relative to its parent Chinese strain  
66 SA14, the largest number, namely 8 were located within the envelope glycoprotein E [4, 5].  
67 Similarly, 8 of the 22 amino acid changes in YF17D relative to its parent Asibi strain were  
68 found in the E protein [6]. Studies in the mouse model implicated multiple mutations within  
69 the E gene of SA14-14-2 in the attenuated phenotype of this vaccine strain [7-10]. Additionally,  
70 a silent G to A mutation near the beginning of the NS2A gene which led to abrogation of -1  
71 ribosome frameshifted NS1' synthesis was reported to determine loss of neurovirulence of  
72 SA14-14-2 [11]. Both viral E and NS1' are secreted glycoproteins synthesized on endoplasmic  
73 reticulum (ER)-bound ribosomes, that are dependent on the ER lumen for glycosylation and  
74 folding. The molecular mechanisms underlying the attenuation caused by these mutations have  
75 not been elucidated.

76 As obligate intracellular parasites, viruses rely on usurping the host translational  
77 machinery for their survival and propagation. The dominant immediate host response to viral

78 infection is a transient shutdown of translation, which serves to limit viral protein synthesis  
79 [12]. PKR-like ER resident kinase (PERK), one of the three ER resident stress sensors which  
80 attenuates translation via phosphorylation of the downstream eukaryotic translation initiation  
81 factor eIF2 $\alpha$  constitutes one of the earliest pathways that responds to the increased burden of  
82 viral protein synthesis within the ER. PERK activation was reported to have divergent effects  
83 on replication of viruses; whereas activated PERK negatively regulated Transmissible  
84 Gastroenteritis Virus (TGEV) replication [13], translation of dengue proteins in mosquito cells  
85 continued despite PERK activation which in fact prolonged survival of infected cells,  
86 ultimately aiding viral replication [14]. Inhibition/degradation of its cytoplasmic counterpart  
87 PKR by multiple viruses to aid their survival and replication has been extensively documented  
88 [15-21]. Sustained phosphorylation of eIF2 $\alpha$  and the resultant translation block is known to  
89 activate autophagy [22]. Several viruses have evolved mechanisms both to prevent  
90 phosphorylation of eIF2 $\alpha$  and leverage autophagy for their own benefit. Influenza A virus,  
91 coxsackie B virus and rotavirus have all evolved to increase autophagy flux and utilize  
92 autophagosomal membranes to facilitate their replication while simultaneously preventing the  
93 antiviral effects of late stages of autophagy maturation and lysosome fusion of autophagosomes  
94 [reviewed in [23]]. Thus, viruses escape completion of autophagy and its attendant activation  
95 of inflammation leading to efficient priming of cytolytic CD8<sup>+</sup> T cells. Autophagy has been  
96 demonstrated to facilitate efficient transporter of antigenic peptide (TAP)-independent  
97 presentation of viral antigenic peptides contained within autophagolysosomes by fusion with  
98 endosomes containing internalized MHC Class I molecules [24].

99 The most conserved ER stress sensor IRE-1 $\alpha$ , an ER transmembrane kinase and  
100 endoribonuclease which is activated when unfolded proteins accumulate within the ER, serves  
101 to match protein folding burden within the ER with capacity. IRE-1 $\alpha$  generates the  
102 transcription factor XBP-1 [25] through nonconventional cytoplasmic splicing which in turn

103 helps to maintain ER homeostasis and prevent activation of cell death pathways caused by  
104 sustained ER stress. The IRE-1 $\alpha$ -XBP-1 axis was reported to be vital and essential for  
105 development and survival of dendritic cells [26], certain subsets of which were shown to  
106 constitutively activate the IRE-1 $\alpha$ -XBP-1 pathway [26, 27]. More importantly, both  
107 transcription and splicing of XBP-1 mRNA were reported to be increased in response to viral  
108 or bacterial infection within antigen specific CD8<sup>+</sup> T cells, whose differentiation into killer cell  
109 lectin-like receptor G1 (KLRG1)-expressing terminal effector cells was dependent on XBP-1  
110 expression [28]. Thus, IRE-1 $\alpha$  is poised to link infection-induced ER perturbation and unfolded  
111 protein response (UPR) to subsequent steps of antigen presentation and generation of host-  
112 protective immune responses.

113 In order to understand the molecular mechanisms by which mutations in E and NS1'  
114 glycoproteins of JEV contribute to the attenuation and immunogenic efficacy of SA14-14-2,  
115 we compared markers of ER stress, UPR and death pathways in cells infected with the WT  
116 (P20778) and vaccine (SA14-14-2) strains of JEV. Our results highlighted the role of JEV NS1'  
117 in orchestrating dephosphorylation of phosphor e-IF2 $\alpha$  by modulating both upstream kinase  
118 PERK and feedback dephosphorylation by CAAT/enhancer binding protein (CEBP)  
119 homologous protein (CHOP) to achieve efficient viral protein synthesis. Sluggish folding  
120 kinetics of SA14-14-2 E protein and the resultant aggravated and unresolved ER protein folding  
121 strain led to enhanced autophagy in SA14-14-2 infected cells. The consequent efficient cross  
122 presentation of viral antigen-containing autophagic vesicles most likely resulted in the  
123 observed augmented activation of antigen presenting cells by SA14-14-2 and enhanced recall  
124 CD8<sup>+</sup> T cell responses to viral structural proteins envelope and capsid in individuals vaccinated  
125 with SA14-14-2.

## 126 **RESULTS**

### 127 **Differential modulation of PERK-eIF2 $\alpha$ -CHOP pathway by wild type and vaccine strains** 128 **of JEV.**

129 As a first step to query the underlying basis for attenuation of SA14-14-2 we compared  
130 activation of the ER stress sensor PERK in JEV-infected cells. We observed progressive  
131 reduction in levels of total and phosphorylated PERK in Neuro2A (N2A; Fig 1A, S1Fig D) as  
132 well as porcine kidney fibroblasts (PS; S1 Fig A) along with rapid dephosphorylation of eIF2 $\alpha$   
133 in both cell lines following infection with P20778 (Fig 1B, S1 Fig E, B and C). Infection with  
134 SA14-14-2 in contrast, led to sustained increase in phosphorylation of eIF2 $\alpha$  in both cell lines  
135 (Fig 1B, S1 Fig B, C and E). We also observed impressive upregulation of CHOP which  
136 mediates induction of the regulatory subunit of the phosphatase responsible for eIF2 $\alpha$   
137 dephosphorylation, accompanied by the transcription factor ATF4, only in cells infected with  
138 P20778 (Fig 1C and D, S1Fig F). CHOP and ATF4 upregulation in the absence of eIF2 $\alpha$   
139 phosphorylation, required to override the upstream ORF in the CHOP and ATF4 mRNA [29]  
140 was intriguing; we did not investigate a potential role for the reported phosphorylation of eIF4E  
141 [30] in CHOP expression. Thus, wild type JEV efficiently prevented the phosphor-eIF2 $\alpha$ -  
142 mediated translation block triggered by the host upon viral infection by destroying upstream  
143 PERK and stimulating downstream feedback expression of CHOP to facilitate viral protein  
144 synthesis. Interestingly, the ER stress sensor IRE-1 $\alpha$  revealed phosphorylation-mediated  
145 activation only in SA14-14-2-infected cells, accompanied by enhanced expression of XBP-1  
146 (Fig 1E, S1 Fig G and H), pointing to increased protein folding stress and activation of UPR  
147 following infection with SA14-14-2 but not P20778.

### 148 **JEV NS1' activates CHOP expression**

149 To query a role for NS1' (absent in SA14-14-2) in modulating the PERK pathway, we created  
150 cells stably expressing NS1 or NS1' of P20778 by lentivirus transduction. PS cells stably  
151 expressing NS1' revealed constitutive high expression of CHOP (Fig 2, lanes 9 to 12). Cells  
152 expressing P20778 NS1 protein were distinctly devoid of CHOP, even on long exposure (Fig  
153 2, lanes 5 to 8). Surprisingly, NS1'-induced CHOP expression did not lead to  
154 dephosphorylation of eIF2 $\alpha$ , presumably due to vital compensatory pathways in cells  
155 conditioned to constitutively express CHOP over multiple passages. We also observed  
156 progressive loss of PERK levels in NS1'-expressing cells over a span of 36 hours (Fig 2, lanes  
157 9 to 12). These results revealed a role for the C-terminal frameshifted 52 amino acid segment  
158 of NS1' in modulating levels of CHOP and PERK following viral infection. Loss of NS1' in  
159 SA14-14-2-infected cells would understandably cripple the vaccine strain due to its inability  
160 to appropriate the translation machinery of the host.

#### 161 **WT JEV blocks autophagy maturation.**

162 The sustained high phosphorylation levels of eIF2 $\alpha$  in SA14-14-2-infected cells led us to  
163 investigate autophagy. Diverse reports exist, of the positive as well as negative effect of  
164 autophagy on JEV replication [31, 32]. P20778 induced impressive stabilization and  
165 consequent increased levels of lipidated LC3-II and p62 beyond 16 h of infection, not seen for  
166 SA14-14-2 (Fig 3A, S2 Fig C and D). In contrast we observed progressive loss of Beclin-1, a  
167 crucial protein required to generate the autophagy maturation complex in P20778-, but not  
168 SA14-14-2-infected PS cells (S2 FigA). Thus, wild type JEV appears to block autophagy  
169 maturation by targeting Beclin in a manner reminiscent of influenza A virus whose M2 protein  
170 directly interacts with Beclin to disrupt the autophagy maturation complex [33]. We then  
171 queried any changes in autophagy flux in virus infected cells using the inhibitor bafilomycin.  
172 Addition of bafilomycin stabilized and increased LC3-II levels in P20778-infected cells at early  
173 times post infection, revealing a modest increase in autophagy flux at 12 and 24 h post infection



174 (Fig 3B, compare lanes 3 and 4 with 13 and 14, S2 FigE). A role for autophagy early during  
175 JEV infection was also reported previously [31]. However, we observed no further stabilization  
176 in levels of LC3-II by bafilomycin over that already achieved by WT-JEV beyond 24 h post  
177 infection (Fig 3B, compare lanes 5 and 6 with 15 and 16, S2 FigE). In contrast, bafilomycin  
178 revealed impressive and sustained increase in autophagy flux within cells infected with SA14-  
179 14-2 (Fig 3B, compare lanes 8 to 10 with 18 to 20, S2 FigE), corroborated by increased levels  
180 of ATG5 and ATG7 (Fig 3C). Thus, WT JEV while increasing autophagy during early stages  
181 of replication, clearly prevented autophagy maturation and late-stage degradative loss of LC3-  
182 II and p62. Such a strategy would provide JEV with the ER-derived membranes that host the  
183 viral replicase complex [34-36] while at the same time preventing the autophagy-induced  
184 efficient priming of virus-specific CD8<sup>+</sup> T cells [23]. This ability to commandeer the host  
185 autophagy pathway was obviously lost during attenuation of SA14-14-2; activated autophagy  
186 flux in SA14-14-2-infected cells is perhaps triggered by persistently phosphorylated eIF2 $\alpha$   
187 [22]. We did not observe alterations in levels of LC3-II or p62 in cells stably expressing NS1'  
188 (data not shown). The viral protein(s) responsible for stabilization of LC3-II and p62 and the  
189 mutation(s) in SA14-14-2 responsible for abrogating this effect are yet to be determined.

190 We then investigated other death pathways in JEV-infected cells. While P20778 did not  
191 affect caspase-3 activation, we observed definitive suppression of residual caspase-3 cleavage  
192 in SA14-14-2-infected cells (Fig 3D, S2 FigF). P20778 infected cells revealed on the other  
193 hand, enhanced phosphorylation of MLKL, indicating early commitment to necroptosis  
194 following WT JEV infection (Fig 3E, S2 FigG). Both viruses also induced over expression of  
195 PARP-1 protein with minor and comparable enhancement of PARP-1 cleavage (S2 FigB).

## 196 **Differential stability of envelope proteins of WT and vaccine strains of JEV**

197 The observed persistent eIF2 $\alpha$  phosphorylation combined with IRE-1 $\alpha$  activation and increased  
198 autophagy flux pointed to unresolved protein folding stress within SA14-14-2-infected cells.  
199 We therefore investigated levels of ER chaperones in virus infected cells. We observed  
200 dramatic upregulation of BiP and calnexin/calreticulin only in SA14-14-2-infected PS and  
201 N2A cells (Fig 4A and B). Keeping in mind the eight mutated residues of SA14-14-2 envelope,  
202 we proceeded to probe the stability and folding of envelope protein in cells infected with JEV.

203 We utilized a rabbit polyclonal antiserum specific to JEV E protein to determine the  
204 half-life of E in cells infected with P20778 and SA14-14-2 strains of JEV. While WT E  
205 displayed a half-life of 5.9 h (S3 FigA, lanes 2 to 8; S3 FigB), SA14-14-2 E was rapidly  
206 degraded with half-life of 1.2 h pointing to its inherent instability (S3 FigA, lanes 9 to 15; S3  
207 FigC). This was borne out by loss of conformational epitopes of SA14-14-2 E upon treatment  
208 with 7 M urea in contrast to P20778 E (S4 FigA). 7 M urea treatment did not affect reactivity  
209 of linear epitopes of SA14-14-2 E recognized by mAb CE3, F4B, DF4 and D10A, while that  
210 to conformational epitopes was lost (S4 FigA, lane 6) with the exception of 2D5. Reduction of  
211 proteins with DTT led to loss of all conformational epitopes in P20778 E protein also (S6 FigA,  
212 lane 3), with 1A5 and 2A9 being exceptions, indicating reliance on disulphide bond formation  
213 for generation of most of the conformational epitopes of E. A defect/delay in formation of  
214 disulphide bonds during the folding of SA14-14-2 E protein was evident from these  
215 observations. Following a short 5 min metabolic labeling of P20778-infected cells, use of N-  
216 ethyl maleimide to alkylate free sulfhydryl groups from the twelve cysteine residues of DTT-  
217 reduced nascent E protein to trap various folding intermediates revealed a fully reduced (R1)  
218 and two distinct intermediate forms (Ri and R2) along with a fully oxidized form (Ox) of E,  
219 the latter confirmed by H<sub>2</sub>O<sub>2</sub> treatment (S4 FigB, lane 2). The rabbit polyclonal serum failed  
220 to immunoprecipitate the alkylated fully reduced form, presumably owing to occlusion of  
221 epitopes by alkylation (compare panels IP and Lysate in S4 FigB, lanes 3 to 8).

222 NEM alkylation of JEV-infected cell monolayers after 15 min of metabolic labeling  
223 revealed that in contrast to P20778 E, nascent SA14-14-2 E protein remained in various  
224 reduced forms for a much longer period post synthesis (S4 FigC). Each of the monoclonal  
225 antibodies mentioned above did indeed recognize its cognate epitope on the different  
226 reduced/oxidized forms of SA14-14-2 E protein (S4 FigC). The differential preference of the  
227 monoclonal antibodies for recognizing the different reduced and single oxidized form of SA14-  
228 14-2 E protein was also evident. More importantly, we also observed that several envelope-  
229 specific linear and conformational epitopes detected on extracellular virus particles of P20778  
230 were missing on SA14-14-2 particles with the exception of the linear epitope recognized by  
231 D10A (S4 FigD).

### 232 **Belated folding kinetics of mutated SA14-14-2 envelope protein**

233 We resorted to direct electrophoresis of labeled and alkylated infected cell lysates to follow the  
234 folding of E protein owing to poor ability to immunoprecipitated alkylated forms by the  
235 polyclonal anti-E serum (S4 FigB). Use of AMD prevented label incorporation into host  
236 proteins, allowing unambiguous visualization of the various forms of E (S4 FigB, lower panel).  
237 The E protein of JEV is co-translationally secreted into the lumen of the ER where it undergoes  
238 oxidation of its twelve cysteine sulfhydryl groups during folding. Wash out of DTT used to  
239 reduce metabolically labeled nascent E protein resulted in rapid oxidation (Ox) of cysteine  
240 sulfhydryl groups of fully reduced R1 form of P20778 E protein through an intermediate  
241 partially reduced species R2 (Fig 5A), leading to 45 % of the nascent protein being converted  
242 to the Ox form within 30 min of DTT removal (Fig 5A, lane 9). The precursor to product  
243 relationship of R1 and Ox forms of E through the intermediate R2 form was evident (Fig 5A,  
244 lanes 3 to 11; S6 FigB). In contrast, we saw a mere 19 % of label in the oxidized form of SA14-  
245 14-2 E protein at 30 min post DTT removal (Fig 5B, lane 9). Substantial proportion of labeled  
246 E protein remaining in the abundant fully reduced R1 form was in fact evidently degraded

247 within this time, elevating the proportion of the scant quantity of Ox form of E. This dramatic  
248 instability of the reduced forms R1 and R2 of SA14-14-2 E was evident when band intensities  
249 were quantitated, with 80 % loss over a span of 60 min (S6 FigC), contributing to the observed  
250 short half-life of SA14-14-2 E protein (S3 Fig). It is to be noted that other viral proteins such  
251 as cytoplasmically localized NS3 and NS5 of SA14-14-2 were not similarly degraded (S5  
252 FigB). Importantly, data in Fig 3B reveals that the ER lumenally localized NS1 protein of  
253 SA14-14-2 is also spared from degradation observed for E, suggesting that the SA14-14-2 E  
254 was specifically targeted presumably by ER-associated degradation (ERAD) machinery of  
255 infected cells owing to its tardy folding kinetics. We observed no such differential instability  
256 of P20778 E relative to NS3 and NS5 (S5 FigA).

257         When we investigated the susceptibility of nascent E protein to reduction by DTT, we  
258 found rapid acquisition of resistance to DTT-mediated reduction by P20778 E within 15 min  
259 of synthesis (Fig 5C, lane 8; S6 FigD). In contrast, majority of SA14-14-2 E protein molecules  
260 remained susceptible to DTT reduction for at least an hour following its synthesis (Fig 5D,  
261 lanes 4 to 10) by which time, nearly 85 % of molecules vulnerable to reduction were degraded  
262 (Fig 5D, lane 10; S6 FigE). One min post synthesis, while a mere 18 % of WT E could be  
263 reduced to R1, this proportion was 50 % for SA14-14-2 E (Fig 5C and D, compare lanes 5).  
264 By 2 to 5 min post synthesis, nascent P20778 E was almost completely resistant to reduction  
265 to the fully reduced R1 form (Fig 5C, lanes 6,7). In contrast, a third of the residual degradation-  
266 resistant SA14-14-2 E protein could be reduced to R1 form even at 30 min post synthesis (Fig  
267 5D, lane 9). Thus, mutations in the SA14-14-2 E protein rendered it incapable of achieving  
268 rapid oxidation-associated folding within the ER. Brefeldin treatment prior to metabolic  
269 labeling caused no difference in the kinetics of oxidative folding of WT and vaccine E proteins,  
270 testifying to ER as the site of E protein oxidation (data not shown).

#### 271 **Accelerated furin cleavage of SA14-14-2 prM protein**

272 Flavivirus maturation involves low pH-dependent furin mediated cleavage of the prM protein  
273 in the Golgi apparatus during egress [37, 38]. In extracellular virus particles of multiple  
274 flaviviruses, a sizeable proportion of prM has been reported to remain unprocessed by furin  
275 [37, 39, 40]. We observed approximately half the prM protein of extracellular P20778 virus  
276 particles had undergone furin cleavage (Fig 6A, fractions 1 to 4, lower panel). A small  
277 proportion of virus particles with maximum density recovered from the bottom of 70% sucrose  
278 following ultracentrifugation alone revealed complete processing of prM to pr and M (Fig 6A,  
279 fraction 6, lower panel). In contrast, we observed near total cleavage of prM to pr and M on  
280 extracellular SA14-14-2 virus particles with uncleaved prM barely visible even on long  
281 exposure (Fig 6A, lower panel). We surmised that the incomplete folding of the mutated  
282 envelope protein perhaps allowed enhanced access to the furin cleavage site of SA14-14-2 prM  
283 protein, which collectively led to the observed alteration of surface epitopes on virus particles  
284 of SA14-14-2 (S4 FigD). As expected, intracellular prM remained uncleaved in cell lysates of  
285 both viruses (Fig 6B, lower right panel)

### 286 **Enhanced CD8<sup>+</sup> T cell responses in SA14-14-2 vaccinated individuals**

287 In order to ask if the above differences in the cell biology of infection with P20778 and SA14-  
288 14-2 would be reflected in the immune response to the virus, we compared recall T cell  
289 responses in individuals exposed to circulating wild type JEV in endemic regions with those  
290 vaccinated with SA14-14-2. Capsid and E protein-specific T cells were both characterized by  
291 the dominance of CD4<sup>+</sup> over CD8<sup>+</sup> subsets in those naturally infected with circulating WT  
292 strains of JEV (HV and JEV groups; Fig 7A, top and middle panels). Capsid-specific CD4<sup>+</sup> T  
293 cell responses were comparable between naturally infected healthy volunteers (HV) or  
294 recovered JEV patients (JEV) and vaccinated individuals (VAC; Fig 7A, top panel) while  
295 envelope specific CD4<sup>+</sup> T cell responses were elevated in SA14-14-2 vaccinated individuals  
296 (VAC) relative to naturally infected individuals HV or JEV (Fig 7A, middle panel).

297 Importantly, significantly greater percentages of capsid-specific CD8<sup>+</sup> T cells secreting IFN- $\gamma$ ,  
298 TNF- $\alpha$  or MIP-1 $\beta$  including polyfunctional ones were observed in vaccinated individuals  
299 compared to infected HV and recovered JEV patients (Fig 7A, top panel). E-specific CD8<sup>+</sup> T  
300 cells secreting IFN- $\gamma$ , TNF- $\alpha$  and MIP-1 $\beta$  including polyfunctional T cells showed  
301 enhancement in SA14-14-2 vaccinated individuals relative to recovered JEV patients (Fig 7A,  
302 middle panel), in keeping with the earlier reported absence of JEV-specific CD8<sup>+</sup> T cells in  
303 recovered JEV patients [41, 42]. In contrast, we did not observe such enhancement of NS3-  
304 specific T cells in vaccinees compared to naturally infected individuals (Fig 7A, lower panel).  
305 NS3 is known to be the strongest stimulator of human CD8<sup>+</sup> T cells in JEV-endemic cohorts  
306 [42, 43]. IL-2 responses to JEV proteins were relatively weak (data not shown). These results  
307 suggested superior presentation of viral structural proteins to CD8<sup>+</sup> T cells following SA14-  
308 14-2 infection.

309         When we queried the ability of P20778 and SA14-14-2 to stimulate activation of  
310 antigen presenting cells, we observed enhanced death of primary mouse dendritic cells and  
311 human monocyte cell line THP-1 detected by Annexin-V and propidium iodide staining  
312 following 24 h infection by SA14-14-2 compared to P20778 (Fig 7B). In parallel, we also  
313 detected impressive increases in levels of inflammatory cytokines IL-12p40, IL-6 and TNF- $\alpha$   
314 secreted from BMDC infected with SA14-14-2 compared to P20778 (Fig 7C). While we have  
315 not investigated the mode of death in infected cells, the above data suggest that presentation of  
316 viral antigens following infection with SA14-14-2 would be far more efficient relative to  
317 P20778. In light of the robust tropism of multiple mosquito-borne flaviviruses for human  
318 dendritic cells [44-46], we surmised that enhanced autophagy within antigen presenting cells  
319 infected with SA14-14-2 would engender superior cross presentation of viral antigens to CD8<sup>+</sup>  
320 T cells as reported in the mouse model of influenza A virus infection [47].

## 321 **DISCUSSION**

322 Both live attenuated vaccines available for two flaviviral pathogens, namely Yellow Fever 17D  
323 and JEV-SA14-14-2, were developed by serial passages in cultured cells, a process that led to  
324 accumulation of multiple mutations. Identity of and underlying molecular mechanisms  
325 triggered by the specific mutations responsible for their attenuated phenotype can help to  
326 exploit them for rationally developing vaccines against several other viral pathogens. We had  
327 the benefit of previous published studies that attributed the attenuation of SA14-14-2 to  
328 mutations in envelope and NS1' [7-11]. Our previous studies had also revealed that the  
329 strongest correlate of naturally acquired immune protection in JEV-endemic human cohorts  
330 was flavivirus cross reactive CD8<sup>+</sup> cytotoxic T cells secreting IFN- $\gamma$  in addition to other TH1  
331 cytokines such as IL-2 and TNF- $\alpha$  [41-43]. We therefore compared the cell biology of  
332 infections by WT and vaccine strains of JEV in cultured cells and attempted to relate them to  
333 differences in activation of antigen presenting cells as well as human recall T cell responses  
334 induced by the two strains of JEV. This rewarding exercise using simple approaches revealed  
335 the role of JEV NS1' protein that is missing in SA14-14-2 in expropriating the host cell's  
336 translational machinery to achieve efficient synthesis of viral proteins. NS1' accomplished this  
337 by maintaining eIF2 $\alpha$  in the dephosphorylated state both by upstream PERK destruction and  
338 downstream CHOP-mediated dephosphorylation. Increased levels of CHOP in JEV RP-9  
339 infected BHK-21 and NT-2 cells was reported previously [48]. CHOP protein translation from  
340 its upstream ORF-containing mRNA requires the presence of phosphorylated eIF2 $\alpha$  [29, 49].  
341 The dramatically increased levels of CHOP in P20778-infected cells even in the absence of  
342 phosphorylated eIF2 $\alpha$  is therefore surprising. Independent expression using lentiviral  
343 transduction confirmed NS1' as the mediator of this phenomenon. The host proteins that NS1'  
344 might interact with and the mechanism by which it upregulates CHOP expression await  
345 unraveling by future investigations. JEV NS4B was earlier reported to activate PERK by



346 inducing its dimerization, leading to apoptosis and thereby encephalitis in mice [50]. That JEV  
347 targets PERK via multiple viral proteins in different tissues testifies to the importance of PERK  
348 in orchestrating both pro- and antiviral mechanisms in response to JEV infection. The reported  
349 reduction of JEV-induced apoptosis brought about by PERK inhibitor GSK2606414 in this  
350 study suggests that NS1' may also serve to mitigate damage to neuronal cells caused by NS4B-  
351 induced PERK activation.

352 Most successful pathogens modulate death pathways in infected cells to escape host  
353 protective immune responses [51, 52]. Inhibition of autophagy to subvert host-protective  
354 immunity is a common strategy adopted by multiple pathogens through varied mechanisms  
355 [23]. WT JEV specifically prevented autophagy maturation leading to dramatic stabilization of  
356 LC3-II and p62 during late stages of infection while increasing autophagy during early phase  
357 of infection as also reported previously [31]. The stabilization of LC3-II at 48 but not 24 hrs  
358 post infection of N2A cells with JEV was also evident in Fig 3A of an earlier study [32]. The  
359 progressive loss of Beclin in P20778-infected PS cells suggests that JEV targets Beclin to  
360 prevent formation of autophagy maturation complex as reported for influenza A virus also [33].  
361 Increased MLKL phosphorylation pointed to necroptosis in WT JEV infected cells. In light of  
362 the reported ability of the autophagosomal component p62 in recruiting RIPK1, leading to  
363 necrosome assembly in association with the autophagy machinery [53], necroptosis in WT JEV  
364 infected cells may be assisted by the observed p62 accumulation. In contrast, the enhanced  
365 autophagy in SA14-14-2 infected cells is most likely triggered by sluggish folding of E, with  
366 resultant unresolved UPR evidenced by high levels of ER chaperones and persistent eIF2 $\alpha$   
367 phosphorylation. These dramatic differences in death pathways activated by WT and vaccine  
368 strains of JEV would undoubtedly alter the host immune response to the two virus strains.  
369 Autophagy within antigen presenting cells has been reported to enhance cross presentation of  
370 viral antigens to prime CD8<sup>+</sup> T cells [47]. Another study also proposed that autophagy-



371 dependent antigen presentation on endocytosed cell surface MHC class I relies on TAP-  
372 independent vacuolar pathway where the acidic autophagolysosomal compartment would  
373 potentially stabilize MHC-peptide complexes [24, 54]. Since numerous viral immune evasion  
374 mechanisms target the TAP-dependent pathway of antigen presentation to escape CD8<sup>+</sup> T cell-  
375 mediated antiviral immunity, autophagy dependent antigen presentation by MHC class I  
376 molecules allows circumventing this conventional pathway to achieve efficient priming of  
377 CD8<sup>+</sup> T cells. The attenuating mutations in SA14-14-2 appear to have attained this outcome by  
378 disabling the WT virus's mechanism(s) for inhibiting autophagy maturation. We therefore  
379 explored mechanisms instigated by mutations in the envelope protein of SA14-14-2 to enhance  
380 autophagy.

381         The retarded folding kinetics brought about by the numerous mutations in E of SA14-  
382 14-2 along with the observed accelerated furin cleavage of SA14-14-2 prM, culminated in  
383 dramatically altered surface epitopes on extracellular virus particles of SA14-14-2. We  
384 leveraged a panel of monoclonal antibodies that recognize several conformational and linear  
385 epitopes on JEV E along with alkylation of metabolically labeled nascent envelope protein to  
386 query the stability and folding kinetics of wild type and vaccine E proteins. The use of AMD  
387 to suppress host translation in virus-infected cells allowed us to effectively visualize and  
388 resolve the three different reduced forms along with oxidized form of the flaviviral E protein  
389 for the first time. The fully reduced R1 and oxidized forms of E revealed a clear precursor-  
390 product relationship during its folding, transiting through intermediate reduced (Ri) and a  
391 partially oxidized/reduced form R2. In addition to delay in folding of nascent SA14-14-2 E  
392 protein, we also observed continued vulnerability of its oxidized form to reduction by DTT for  
393 nearly an hour after synthesis; the P20778 E protein in contrast achieved DTT resistance in 5  
394 min post synthesis. Failure of the mutated SA14-14-2 E protein to efficiently attain the stable  
395 oxidized form despite induction of ER chaperones BiP and calnexin/calreticulin probably

396 resulted in its rapid degradation, most likely by the ER-associated degradation (ERAD)  
397 pathway. The acute stress inflicted on the ER protein folding machinery by mutated E of SA14-  
398 14-2 appears to be the immediate cause of autophagy enhancement mediated by persistent  
399 eIF2 $\alpha$  phosphorylation. The abundant levels of viral NS proteins 1, 3 and 5 in SA14-14-2  
400 infected cells (Fig 3B, S1 FigA) would suggest that despite IRE-1 $\alpha$  activation, viral mRNA  
401 degradation by regulated IRE-1 $\alpha$  dependent decay (RIDD) was not triggered. Among these NS  
402 proteins, it is particularly notable that NS1 of SA14-14-2 escapes degradation despite being  
403 ER localized (Fig 3B), further confirming that the targeted susceptibility of SA14-14-2 E to  
404 degradation emanates from its delayed folding kinetics within the ER.

405 We suspect that the unstable conformation of SA14-14-2 E protein permits superior  
406 access for golgi-resident furin to the prM protein in the immature viral particles on their exit  
407 path to the cell's exterior. Extracellular virus particles of both JEV and WNV were shown to  
408 carry substantial proportions of uncleaved prM protein [39, 40]. Elegant cryo-electron  
409 microscopy studies combined with immunoprecipitation of metabolically labeled extracellular  
410 dengue virus particles with envelope and pr-specific antibodies revealed 30 to 40 % uncleaved  
411 prM distributed on 90 % of total virus particles, giving rise to a sizeable proportion of “partially  
412 mature” structurally dynamic virus particles [37]. The conformational flexibility and size  
413 heterogeneity of virus particles which was modulated by prM cleavage [55] would most likely  
414 permit the particles to “breathe” [56], rendering them difficult to target by the host immune  
415 system [57]. One is tempted to speculate that the near total cleavage of prM to pr and M on  
416 virus particles of SA14-14-2 that we observed, would likely give rise to homogeneous virus  
417 particles with rigid conformation that are efficiently targeted by host immune mechanisms.  
418 Furin cleavage of prM along with the acidic trans golgi environment are prerequisites for  
419 converting the intracellular immature ‘spiky’ virus particles into a flattened conformation of  
420 smooth mature particles [38, 58]. Structure investigations of SA14-14-2 virus particles ought

421 to clarify whether the nearly complete prM cleavage renders these particles smooth and  
422 homogeneous in appearance.

423 The observed significantly higher levels of inflammatory cytokines from primary  
424 BMDC infected with SA14-14-2 as well as significantly greater death of infected BMDC and  
425 THP-1 human monocytes compared to P20778, most likely resulted from the enhanced  
426 autophagy triggered by SA14-14-2. This ability of SA14-14-2 to better activate BMDC was  
427 also evident when comparing two earlier reports [59, 60]. In keeping with this observation, we  
428 also noted enhanced CD8<sup>+</sup> T cell responses directed to the structural proteins envelope and  
429 capsid of JEV in SA14-14-2 vaccinated individuals. The localization of capsid and envelope  
430 which are tethered to the ER membrane, would allow them access to the autophagy vesicles  
431 that are ER membrane derived [61, 62] and thus permit effective cross presentation to CD8<sup>+</sup> T  
432 cells. This pathway would not be available for the cytoplasmically localized NS3, the dominant  
433 target of CD8<sup>+</sup> T cells during natural infections, explaining the observed comparable NS3-  
434 specific T cell responses between naturally infected and vaccinated individuals. It is to be noted  
435 that the elevated CD8<sup>+</sup> T cells were not evident in vaccinated individuals within the first 6  
436 weeks post vaccination [63], suggesting efficient memory T cell generation following SA14-  
437 14-2 infection. It may be argued that these differences in CD8<sup>+</sup> T cells between vaccinated and  
438 naturally infected individuals might merely reflect the time elapsed since infection. We cannot  
439 precisely determine the time of last exposure in naturally infected individuals residing in JEV-  
440 endemic regions. In fact, at the time of our sampling, JEV circulation was evident from the  
441 large number of hospitalized JE patients, suggesting that the lower levels of CD8<sup>+</sup> T cells in  
442 naturally infected individuals was unlikely due to longer time elapsed between exposure to JEV  
443 and sampling. Our earlier studies revealed that during human infection with circulating strains  
444 of JEV, envelope protein predominantly stimulates CD4<sup>+</sup> T cells with little evidence for CD8<sup>+</sup>  
445 T cells [42]. WT JEV clearly possesses effective mechanisms to abort the generation of host-

446 protective immune responses, including by suppressing the maturation of autophagic vesicles.  
447 Our results indicate that necroptosis induced by wild type JEV most likely suppressed  
448 presentation of CD8<sup>+</sup> epitopes in the envelope and capsid proteins as also reported in HIV  
449 progressors [64], while the shift to autophagy induced by SA14-14-2 promoted cross  
450 presentation of these same epitopes to efficiently prime CD8<sup>+</sup> T cells. Indeed, WT JEV has  
451 been reported to suppress priming of CD8<sup>+</sup> T cells through the induced secretion of IL-10 by  
452 infected dendritic cells [44]. The use of recombinant envelope and capsid proteins derived from  
453 P20778 in our recall T cell assays testifies to the preservation of E-derived CD8<sup>+</sup> epitopes in  
454 SA14-14-2 despite the multiple mutations. Thus, our findings throw light not only on  
455 mechanisms underlying the vaccine efficacy of SA14-14-2 but also illuminate the host  
456 immunity-subverting strategies adopted by WT JEV.

457         The development of existing live attenuated viral vaccines by serial passages of viral  
458 pathogens in cultured cells rendered it difficult to pinpoint those mutations that dictate the  
459 attenuated phenotype. The dominant attenuating effect of the envelope mutations revealed by  
460 substituting the envelope gene of wild type India78 strain of JEV with that from SA14-14-2  
461 [7], suggests that defective folding of viral glycoproteins and the ensuing unresolved ER stress  
462 can sufficiently alter the cell biology of infection and antigen presentation to guarantee vaccine  
463 efficacy. The emphasis on JE virus neutralizing antibody titer for 50 % virus neutralization  
464 (PRNT50) of  $\geq 10$  as a sole surrogate of protection [65] led to a dearth of literature  
465 documenting T cell responses to JEV proteins in recipients of various JEV vaccines including  
466 SA14-14-2 [63]. Consequently, we know little about the extent to which vaccine-elicited CMI  
467 responses contribute to vaccine efficacy or reflect those seen in endemic settings. Interestingly,  
468 mice immunized with ChimeriVax-JE, in the complete absence of YFV-neutralizing  
469 antibodies, were protected against YFV challenge, confirming the autonomous protective  
470 ability of flavivirus-specific CMI responses [66] perhaps aided by non-neutralizing envelope

471 specific antibodies. Conversely, the ability of neutralizing antibodies elicited by the mutated  
472 envelope of SA14-14-2 to effectively neutralize circulating wild type strains of JEV deserves  
473 scrutiny.

## 474 **MATERIALS AND METHODS**

### 475 **Cell lines and viruses**

476 Mouse neuroblast cell line Neuro-2a (CLS # 400394/p451\_Neuro-2A, RRID:CVCL\_0470)  
477 *Aedes albopictus* cell line, C6/36 (ATCC # CRL-1660, RRID:CVCL\_Z230) and porcine  
478 kidney fibroblast cell line PS [67], obtained from the National Centre for Cell Science, Pune,  
479 India were grown in minimum essential medium (MEM; Gibco #41500-018) supplemented  
480 with 5% fetal bovine serum (FBS; Gibco #11573397). THP-1 human monocyte cells from  
481 American Type Culture Collection (ATCC) were maintained in RPMI 1640 medium (Gibco  
482 #11500456) with 10% heat inactivated FBS. Bone marrow derived dendritic cells were  
483 obtained by differentiating bone marrow cells from 6 week old BALB/c mice as described [68]  
484 and infected with JEV strains at a multiplicity of 1.

485 JEV strain P20778, West Nile Virus strain E101 (National Institute of Virology, Pune, India)  
486 and SA14-14-2 (Chengdu Institute of Biological Products, Chengdu, Sichuan, China) were  
487 propagated in the *Aedes albopictus* cell line, C6/36 or Neuro-2a cells infected at a multiplicity  
488 of infection (m.o.i) of 0.02. Virus stocks were harvested from the former after 6 days; P20778  
489 and SA14-14-2 were harvested from the latter 72 and 96 hours post infection (h.p.i),  
490 respectively. Virus titres were determined by plaque assay on PS cells infected with serial  
491 dilutions of virus stocks; monolayers were stained with 1 % crystal violet in 20 % ethanol-  
492 water 72 to 96 h.p.i.

### 493 **Ethics Statement**

494 This study was performed in accordance with the principles of the declaration of Helsinki. The  
495 study was approved by the IISc Institutional Human Ethics Committee (ref 5/2011).  
496 Vaccination of healthy volunteers with SA14-14-2 was registered at clinicaltrials.gov  
497 (<https://clinicaltrials.gov/ct2/show/NCT01656200>).

#### 498 **Participants**

499 Recovered JEV patients (JEV; N= 17) were recruited at dedicated outpatient clinics held at the  
500 Vijayanagar Institute of Medical Sciences, Bellary, Karnataka while healthy donors (HV;  
501 N=10) were drawn from family members of patients and members of the local community as  
502 previously reported [42]. Healthy adults recruited by word of mouth and advertisement in  
503 Bangalore and vaccinated with SA14-14-2 (VAC; N=9) as reported earlier [63] were also used  
504 for this study. Patients and vaccinees were bled once 10 to 12 months post  
505 discharge/vaccination.

#### 506 **Infection of cells and Lysate preparation**

507 PS and N2A cells were infected with JEV strains at a multiplicity of 10 for all  
508 experiments. Pre-warmed growth medium was changed completely every 8 h. Cells were  
509 harvested by scraping the monolayer. Cell pellets were lysed in ice cold lysis buffer (20 mM  
510 Tris- HCl pH 7.5, 50 mM sodium pyrophosphate, 50 mM NaF, 150 mM NaCl, 1 mM EDTA,  
511 1 mM EGTA, 100  $\mu$ M Na<sub>3</sub>VO<sub>4</sub>, 1 % Triton X-100) for 15 min. Lysates were clarified by  
512 centrifugation at 1000 rpm, 4 °C for 10 min and stored at -80 °C.

#### 513 **Western blot analysis**

514 Lysates prepared as mentioned above were electrophoresed on SDS-PAGE, transferred  
515 to nitrocellulose or PVDF membranes and western blotting was conducted using the following  
516 primary antibodies: eIF2 $\alpha$  (Cell Signaling Technology #9722), p-eIF2 $\alpha$  (Cell Signaling  
517 Technology #9721), ATG7 (Cell Signaling Technology #2631), ATG5 (Cell Signaling  
518 Technology #8540), LC3B (Santa cruz #sc-271625),  $\beta$ -actin (Cell Signaling Technology

519 #4967), GAPDH (Santa cruz #sc-47724), CHOP (Cell Signaling Technology #2895S),  
520 Calnexin (Cell Signaling Technology #2679S), PERK (Cell Signaling Technology #3192), BiP  
521 (Cell Signaling Technology #3177), Calreticulin (Rabbit mAb D3E6; Cell Signaling  
522 Technology #12238), PARP-1 (Rabbit mAb 46D11; Cell Signaling Technology #9532),  
523 Caspase-3 (Rabbit mAb 8G10; Cell Signaling Technology #9665), ATF4 (Rabbit mAb D4B8;  
524 Cell Signaling Technology #11815) MLKL (Rabbit mAb D2I6N; Cell Signaling Technology  
525 #14993), pMLKL (phospho S345; Abcam #ab196436), Beclin-1 (Cell Signaling Technology  
526 #3738), IRE-1 $\alpha$  (Novus Biologicals #NB100-2323), XBP-1 (Rabbit Polyclonal; Novus  
527 Biologicals #NBP1-77681), SQSTM1/p62 (D5E2; Cell Signaling Technology #8025 and  
528 rabbit polyclonal; Abcam #ab91526, to detect porcine and murine p62, respectively).  
529 Antibodies to viral proteins E, prM, NS1' (mouse monoclonal), NS3 (rabbit polyclonal) and  
530 NS5 (mouse polyclonal) were generated in house [43, 69]. Membranes blocked for 2 h at room  
531 temperature with 0.5% non-fat milk powder (Carnation) in TBS buffer (10 mM Tris pH-8, 150  
532 mM NaCl) were incubated with primary antibody in TBS overnight at ambient temperature.  
533 Membranes were washed thrice with TBS/ 0.1% Tween20, incubated with appropriate  
534 secondary antibody in TBS buffer, washed thrice with TBS/ 0.1% Tween20, and developed  
535 using BIO-RAD Clarity western ECL substrate (#170-5060) using ImageQuant™ LAS 4000  
536 from GE healthcare Life Sciences.

### 537 **Cloning of NS1' and NS1 in lentiviral vector**

538 Total RNA obtained from JEV P20778-infected PS cells harvested 24 h.p.i. was reverse  
539 transcribed using primer OSV 381 with AMV Reverse Transcriptase (Promega). The JEV NS1  
540 gene was PCR-amplified with Deep Vent polymerase (New England Biolabs) using forward  
541 primer OSV 389 and sequential reverse primers OSV 381, OSV 382, OSV 387, OSV 388, OSV  
542 390 and OSV 391 (Table S1) to obtain the full length NS1' gene. OSV 387 and OSV388 were  
543 designed to disrupt the slippery heptanucleotide and pseudoknot structure at the beginning of



544 the NS2a gene of JEV that promote ribosomal frameshifting, without altering the amino acid  
545 sequence of the NS1' C-terminus. The full length NS1' gene was amplified using forward  
546 primer OSV 389 and reverse primer OSV393 containing the haemagglutinin (HA) tag sequence  
547 followed by a termination codon and a *NotI* site. Cohesive ends were generated by restriction  
548 digestion of this PCR product using *EcoR1* and *Not1* and ligated using T4 DNA ligase  
549 (Promega) with *EcoR1*, *Not1* digested and Calf Intestinal Phosphatase treated pCDH-CMV-  
550 MCS-EF1 $\alpha$ -copGFP Dual Promoter Cloning and Expression Lentivector (System Biosciences  
551 LLC, #CD511B-1). Similarly, cDNA synthesized using reverse primer OSV278 was used to  
552 amplify the NS1 gene along with forward primer OSV389 (Table S1). The PCR product was  
553 digested with *SalI*, Klenow filled and digested with *EcoRI*. Ligation to pCDH-CMV-MCS-  
554 EF1 $\alpha$ -copGFP Dual Promoter Cloning and Expression Lentivector digested with *NotI*, Klenow  
555 filled and *EcoRI* digested was carried out. Recombinant plasmids from transformed *E. coli*  
556 DH10B electrocompetent cells identified by diagnostic restriction digestion were verified by  
557 sequencing. Expression of the authentic NS1' and NS1 proteins in HEK-293T cells transfected  
558 with the recombinant pCDH-NS1'HA and pCDH-NS1 plasmids was confirmed by western  
559 blotting using a monoclonal antibody generated against a peptide sequence derived from the  
560 frameshifted C-terminal sequence of NS1' (see below) which specifically detected NS1' in  
561 P20778-infected cells and a polyclonal serum raised to *E. coli* expressed recombinant JEV-  
562 NS1 protein [43], respectively.

### 563 **NS1 and NS1' Lentivirus Generation**

564 293T/17 cells were transfected with pCDH-NS1'HA or pCDH-NS1 along with the  
565 three packaging plasmids psPAX, pVSV-G and pRSV-rev using calcium phosphate. Briefly,  
566 0.6 million 293T/17 cells were seeded on 35 mm dish (BD Falcon) in 2 ml MEM, 5 % FBS.  
567 One day later, medium was changed one hour prior to transfection and fresh 1.8 ml complete  
568 MEM was added. Transfection mix containing the four plasmids in 50  $\mu$ l autoclaved water, 50



569  $\mu$ l 2.5 M calcium chloride and 100  $\mu$ l 2X HEPES buffered saline was immediately added onto  
570 the 293T/17 cells drop by drop. Brief centrifugation for 120 s at 1000 rpm in a swing out rotor  
571 was carried out to enable rapid sedimentation of precipitates. 4 h post transfection, medium  
572 was changed with pre-warmed complete MEM. Supernatant collected 4 days post transfection  
573 was stored at -80 °C. p24 ELISA was performed to determine the lentivirus titer using Perkin  
574 Elmer p24 ELISA kit (#NEK050001KT) according to manufacturer's instructions.

### 575 **Monoclonal antibody generation**

576 To generate NS1'-specific monoclonal antibody a peptide sequence was derived from the C-  
577 terminal frameshifted segment of NS1' protein (SQEVDGQIDHSCGFG) using Bcepred  
578 software (<http://crdd.osdd.net/raghava/bcepred/>) based on hydrophilicity, flexibility,  
579 accessibility, exposed surface, polarity and antigenic propensity. The peptide was conjugated  
580 to BSA using glutaraldehyde and used to immunize BALB/c mice (50  $\mu$ g each per mouse, 3  
581 times at 4-week intervals). To generate antibodies against JEV/WNV envelope/premembrane  
582 proteins, BALB/c mice were injected intraperitoneally with  $2 \times 10^6$  pfu of virus. Subsequently,  
583 two boosters with  $2 \times 10^6$  pfu of virus were administered at intervals of 30 days. 7 days post  
584 injection of each booster, sera were collected by retro-orbital bleeding and tested by western  
585 blotting of JEV-infected cell lysates and ELISA against the peptide with dilutions ranging from  
586 1:1000 to 1:100,000. Spleen cells isolated from the mouse with the best serum titre were fused  
587 with Sp2/0 cells in the ratio of 5:1 using polyethylene glycol (PEG) 3000 (#817019, Merck).  
588 10 million cells of the fusion mix were combined with  $2 \times 10^4$  BALB/c peritoneal macrophages  
589 and seeded in a 96-well plate. Hybridoma were selected in HAT medium for 6 days followed  
590 by HT supplemented medium [70]. Culture supernatants were screened by ELISA on day 10.  
591 Culture supernatants collected from the monoclonal antibody producing cloned cells were  
592 verified by reactivity to authentic NS1'/E/prM in JEV-infected cell lysates by western blotting.

### 593 **Metabolic labelling and immunoprecipitation**

594 Cells were seeded at a density of  $2 \times 10^5$  cells/35 mm dish and cultured for 48 h at 37 °C to  
595 reach 70 % confluence. Cells were infected at a multiplicity of 10 with P20778 or SA14-14-2  
596 at 37 °C for 1 h. Virus inoculum was replaced with pre-warmed complete MEM. 15 h.p.i. for  
597 P20778 and 19 h.p.i. for SA14-14-2 endogenous pools of cysteine and methionine were  
598 depleted by treating cells for 2 h with Cys<sup>-</sup> Met<sup>-</sup> MEM (MP Biomedicals #1641454) containing  
599 7.5 µg/ml Actinomycin-D (AMD; Sigma-Aldrich #A9415) to inhibit host transcription. Cells  
600 were pulsed with 450 µCi/35 mm dish of <sup>35</sup>S-labeled methionine and cysteine (American  
601 Radiolabeled Chemicals, 1175 Ci/mmol; #ARS0110A) diluted in 2 ml MEM, 1 % FBS and  
602 7.5 µg/ml AMD for 5 min. For chase, radiolabel was removed and pre-warmed complete MEM  
603 containing cold 20 mM each of cysteine and methionine was added. Cells were either left  
604 untreated or treated with 100 mM dithiothreitol (DTT) for 5 min, 100 µM hydrogen peroxide  
605 (H<sub>2</sub>O<sub>2</sub>) for 5 min or alkylated with 20 mM N-ethyl maleimide (NEM; Sigma #E3876) in 100  
606 mM sodium phosphate, 150 mM NaCl pH-7.2 (PBS) on ice for 10 min. Monolayers were  
607 harvested by scraping and cell pellets lysed either in lysis buffer (20 mM Tris pH-7.5, 150 mM  
608 NaCl, 1 mM EDTA, 1 mM EGTA, 1 % Triton X-100, 2.5 mM sodium pyrophosphate, 1 mM  
609 beta-glycerophosphate, 1 mM sodium vanadate, 1 mM sodium fluoride, 1X protease inhibitor  
610 cocktail) for electrophoresis on 7.5 % PAGE or in ice-cold RIPA lysis buffer (150 mM NaCl,  
611 1 % Triton X-100, 0.5 % deoxycholic acid) for immunoprecipitation with Protein A/G beads  
612 coated with rabbit polyclonal/mouse monoclonal antibody against envelope protein. Bound  
613 proteins eluted from washed beads using 1X Laemmli SDS-PAGE buffer without DTT at 37  
614 °C for 10 min were electrophoresed in SDS-7.5 % PAGE. Gels were dried in a BIO-RAD  
615 Model 583 gel dryer and developed using the Typhoon FLA 9500 biomolecular imager (GE  
616 healthcare Life Sciences).

617 **ELISA**

618 Peptides were coated at a concentration of 1 µg/ml, 100 µl/ well. 100 µl containing 10<sup>4</sup> pfu of  
619 either P20778 or SA14-14-2 virus in 100 mM carbonate buffer pH-9.6 was coated on high  
620 binding ELISA plates (Orange scientific) and incubated for 12 h at 4 °C in a humidified  
621 chamber. Wells were washed thrice with 100 mM sodium phosphate, 150 mM NaCl, 0.05 %  
622 Tween 20 pH-7.2 (PBST), blocked with 200 µl 0.1 % BSA in 1X PBS and incubated at room  
623 temperature for 2 h. Wells were washed thrice with PBST followed by incubation with 100 µl  
624 of appropriate hybridoma culture supernatant at ambient temperature for 3 h. 100 µl of  
625 horseradish peroxidase (HRP)-conjugated goat anti-mouse secondary antibody (Southern  
626 Biotech #1036-05) was then added at a dilution of 1:5000 and incubated for 1 h at ambient  
627 temperature. Wells were washed thrice with PBST, once with PBS and 100 µl 1X TMB/H<sub>2</sub>O<sub>2</sub>  
628 substrate was added. Reaction was stopped after 30 min using 0.2 N sulphuric acid and  
629 absorbance at 450 nm was obtained using a TECAN Infinite F50 ELISA reader with Magellan  
630 V 7.2 software. Mouse IL-12p40, IL-6 and TNF-α were measured using DuoSet® ELISA kits  
631 (R&D Systems).

632 **Intracellular cytokine detection**

633 Whole, heparinized (sodium heparin) blood was diluted 1:1 with RPMI 1640 and 1 ml aliquots  
634 were stimulated with recombinant NS3, envelope or capsid proteins of JEV P20778 purified  
635 as reported [43] at a concentration of 5 µg/ml for 20 h as described [71]. Brefeldin A (Sigma-  
636 Aldrich #B7651; 10 µg/ml) was added 2 h after peptide addition while monensin (Sigma-  
637 Aldrich #475895) was added 6 h later at a concentration of 0.75 µM, a concentration that we  
638 determined to effectively block secretion of cytokines without adversely affecting cell viability  
639 following 12 h exposure. We used both these secretion inhibitors since they differentially block  
640 surface expression/secretion of several markers studied [72, 73]. 12 h later, erythrocytes were  
641 lysed by addition of 10 volumes of ammonium chloride lysis solution (166 mM ammonium

642 chloride, 9.9 mM potassium bicarbonate and 0.126 mM EDTA), vigorously vortexed for 1 min  
643 and leukocytes retrieved by centrifugation were fixed using 2 % paraformaldehyde (Merck  
644 #158127) on ice for 10 min and washed with PBS-0.1 % sodium azide solution.

645 Cells were then permeabilized with 0.1 % saponin (Merck #47036) and 0.1 % bovine serum  
646 albumin in PBS for 15 min on ice and intracellular cytokines were detected using an antibody  
647 cocktail consisting of titrated amounts of anti-CD3-APC-H7 (SK7), anti-CD8-PerCP (SK1),  
648 anti-IFN- $\gamma$ -PECy7 (B27), anti-IL-2-FITC (MQ1-17H12), anti-TNF $\alpha$ -APC (6401-1111) and  
649 anti-MIP-1 $\beta$ -PE (D21-1351), from BD Pharmingen, San Diego, CA. Data were acquired on a  
650 BD-FACS Canto II flow cytometer (Becton Dickinson, San Jose, CA). Singlet small  
651 lymphocytes were collected after excluding dead cells and debris by gating on forward versus  
652 side scatter and then gated on CD3<sup>+</sup> T lymphocytes. CD3<sup>+</sup> cells negative for CD8 were  
653 considered as CD4<sup>+</sup> T cells (Figure S7). For each analysis, a minimum of 100,000 CD4<sup>+</sup>/CD8<sup>+</sup>  
654 T cell subsets were acquired and data analyzed using FlowJo (Version 7.0 for Windows,  
655 Ashland, Oregon), PESTLE and SPICE [74] software. Antibody-stained unstimulated cells  
656 served as control. A positive response was defined by a minimum number of 50 events over  
657 controls. Gates were positioned to retain the response of unstimulated cells  $\leq$  0.01 % of total  
658 CD4<sup>+</sup>/CD8<sup>+</sup> T cells for IFN- $\gamma$ , TNF- $\alpha$  and IL-2 secreting T cells, while it was  $\leq$  0.05 % for  
659 MIP-1 $\beta$  single cytokine secreting T cells.

#### 660 **Monitoring cell death by flow cytometry**

661 Cells were stained with a combination of Annexin V-FITC (BD Biosciences #556420) and  
662 propidium iodide (BD Biosciences #556463) as described [75]. Cells washed in ice cold PBS  
663 were suspended in binding buffer (10 mM HEPES pH-7.4, 140 mM NaCl, 2.5 mM CaCl<sub>2</sub>) and  
664 stained with a combination of Annexin-V FITC and 250 ng of propidium iodide in 100  $\mu$ l for  
665 30 minutes. Cells were washed in binding buffer, fixed with 2 % paraformaldehyde (Merck

666 #158127) for 10 min on ice, washed with cold PBS and treated with RNase A (0.1 mg/mL;  
667 ThermoFisher Scientific #EN0531) for 15 min at 37 °C before being acquired in a BD-FACS  
668 Canto flow cytometer.

#### 669 **Sucrose gradient centrifugation of JEV**

670 P20778 or SA14-14-2 virus grown on C6/36 cells were overlaid on a cushion of 8 ml 25 %  
671 sucrose and ultracentrifuged at 4 °C for 3 h at 80,000 x g in a Beckman Model L8-70M  
672 ultracentrifuge. Virus pellets resuspended in GTNE (200 mM glycine, 50 mM Tris pH 7.5, 100  
673 mM NaCl, 1 mM EDTA) buffer were overlaid on a sucrose step gradient consisting of 1.5 ml  
674 each of 70 and 30 % sucrose and centrifuged at 4 °C for 3 h at 100,000 x g in a SW60 Ti rotor  
675 in a Beckman Model L8-70M ultracentrifuge. Virus band was observed at the 30-70 % sucrose  
676 interface. 0.5 ml fractions were collected from the 30-70 % sucrose interface until the bottom  
677 of the tube and stored at -80 °C.

#### 678 **Statistical analysis**

679 All western blotting experiments were carried out in biological triplicates. Statistical  
680 analyses were done using GraphPad Prism version 8.0. Significant difference between two or  
681 multiple groups was tested using Mann–Whitney *U* test (two-tailed) and non-parametric  
682 Kruskal-Wallis test with Dunn’s test or parametric ANOVA with Bonferroni correction for  
683 multiple comparisons, respectively. Band intensities quantitated using ImageJ were compared  
684 using unpaired Student's *t* test with alpha set at 0.05.

#### 685 **Acknowledgements:**

686 We thank Sai Pallavi Pradeep and Madhusudan Thirumallesh for help with compiling figures.  
687 We thank Sukanya Raghu for help with Western blots. This study was funded by a grant  
688 (EMR/2016/000373) awarded to VS by the Science and Engineering Research Board,  
689 Department of Science and Technology, Government of India and DBT-IISc Partnership

690 Program Phase-II (BT/PR27952/INF/22/212/2018) awarded to the Biology Division, Indian  
691 Institute of Science. This research was also funded in part, by a Wellcome Trust fellowship  
692 awarded to LT [087757/Z/08/Z], currently funded by Wellcome trust grant number  
693 205228/Z/16/Z. For the purpose of Open Access, the author (LT) has applied a CC BY public  
694 copyright licence to any Author Accepted Manuscript version arising from this submission. LT  
695 is also supported by the National Institute for Health Research Health Protection Research Unit  
696 (HPRU) in Emerging and Zoonotic Infections (NIHR200907) at University of Liverpool in  
697 partnership with Public Health England (PHE), in collaboration with Liverpool School of  
698 Tropical Medicine and the University of Oxford. LT is based at University of Liverpool. The  
699 views expressed are those of the author(s) and not necessarily those of the NHS, the NIHR, the  
700 Department of Health or Public Health England. The funders had no role in study design, data  
701 collection and analysis, decision to publish, or preparation of the manuscript.

## 702 **Author Contributions**

703 VS conceived, designed, planned and executed experiments, supervised the study, curated,  
704 interpreted and visualized data, acquired funds and resources, wrote and edited the manuscript;  
705 LT conceived designed and executed human vaccination studies and acquired funds and  
706 resources; PHV executed experiments, interpreted data, prepared figures and wrote the  
707 manuscript; NK carried out and interpreted experiments, prepared figures; SK and KC carried  
708 out experiments.

709 **Data availability.** All relevant data are within the manuscript and its Supporting Information  
710 files. De-identified flow cytometry files (.fcs) that support the results reported in this article,  
711 have been deposited in Mendeley Data (<https://data.mendeley.com/datasets/2g9jv6bzx5/1>).

712 **Declaration of interests.** The authors declare no competing interests.

713 **REFERENCES**

- 714 1. Uchil PD, Satchidanandam V. Phylogenetic analysis of Japanese encephalitis virus:  
715 envelope gene based analysis reveals a fifth genotype, geographic clustering, and multiple  
716 introductions of the virus into the Indian subcontinent. *Am J Trop Med Hyg.* 2001;65(3):242-  
717 51.
- 718 2. Mitamura T, Kitaoka M, Watanabe M, Okuba K, Tenjin S, Yamada S, et al. Study on  
719 Japanese encephalitis virus. Animal experiments and mosquito transmission experiments.  
720 *Kansai Iji.* 1936;1:260-70.
- 721 3. Campbell GL, Hills SL, Fischer M, Jacobson JA, Hoke CH, Hombach JM, et al.  
722 Estimated global incidence of Japanese encephalitis: a systematic review. *Bull World Health*  
723 *Organ.* 2011;89:766-74E. doi: <http://dx.doi.org/10.2471/BLT.10.085233>. PubMed Central  
724 PMCID: PMC22084515.
- 725 4. Aihara S, Chunming R, Yong-Xin Y, Lee T, Watanabe K, Komiya T, et al.  
726 Identification of mutations that occurred on the genome of Japanese encephalitis virus during  
727 the attenuation process. *Virus Genes.* 1991;5(2):95-109. doi: 10.1007/bf00571925.
- 728 5. Nitayaphan S, Grant JA, Chang G-JJ, Trent DW. Nucleotide sequence of the virulent  
729 SA-14 strain of Japanese encephalitis virus and its attenuated vaccine derivative, SA-14-14-2.  
730 *Virology.* 1990;177(2):541-52. doi: [https://doi.org/10.1016/0042-6822\(90\)90519-W](https://doi.org/10.1016/0042-6822(90)90519-W).
- 731 6. Galler R, Freire MS, Jabor AV, Mann GF. The yellow fever 17D vaccine virus:  
732 molecular basis of viral attenuation and its use as an expression vector. *Brazilian Journal of*  
733 *Medical and Biological Research.* 1997;30(2):157-68. doi: 10.1590/s0100-  
734 879x1997000200002.
- 735 7. Gromowski GD, Firestone C-Y, Whitehead SS. Genetic Determinants of Japanese  
736 Encephalitis Virus Vaccine Strain SA14-14-2 That Govern Attenuation of Virulence in Mice.  
737 *Journal of Virology.* 2015;89(12):6328-37. doi: 10.1128/jvi.00219-15.



- 738 8. Yang H, Fan F, Liu L, Liu J, Sun Y, Xie A, et al. A novel amino acid site closely  
739 associated with the neurovirulence of live, attenuated Japanese encephalitis vaccine (SA14-14-  
740 2 strain). *Vaccine*. 2020. doi: <https://doi.org/10.1016/j.vaccine.2020.01.005>.
- 741 9. Yang J, Yang H, Li Z, Wang W, Lin H, Liu L, et al. Envelope Protein Mutations L107F  
742 and E138K Are Important for Neurovirulence Attenuation for Japanese Encephalitis Virus  
743 SA14-14-2 Strain. *Viruses*. 2017;9(1):20. PubMed PMID: doi:10.3390/v9010020.
- 744 10. Yun S-I, Song B-H, Kim J-K, Yun G-N, Lee E-Y, Li L, et al. A Molecularly Cloned,  
745 Live-Attenuated Japanese Encephalitis Vaccine SA14-14-2 Virus: A Conserved Single Amino  
746 Acid in the *ij* Hairpin of the Viral E Glycoprotein Determines Neurovirulence in Mice. *PLoS*  
747 *Pathog*. 2014;10(7):e1004290. doi: 10.1371/journal.ppat.1004290.
- 748 11. Ye Q, Li X-F, Zhao H, Li S-H, Deng Y-Q, Cao R-Y, et al. A single nucleotide mutation  
749 in NS2A of Japanese encephalitis live vaccine virus (SA14-14-2) ablates NS1' formation and  
750 contributes to attenuation. *Journal of General Virology*. 2012. doi: 10.1099/vir.0.043844-0.
- 751 12. Liu Y, Wang M, Cheng A, Yang Q, Wu Y, Jia R, et al. The role of host eIF2 $\alpha$  in viral  
752 infection. *Virology Journal*. 2020;17(1):112. doi: 10.1186/s12985-020-01362-6.
- 753 13. Xue M, Fu F, Ma Y, Zhang X, Li L, Feng L, et al. The PERK Arm of the Unfolded  
754 Protein Response Negatively Regulates Transmissible Gastroenteritis Virus Replication by  
755 Suppressing Protein Translation and Promoting Type I Interferon Production. *Journal of*  
756 *Virology*. 2018;92(15):e00431-18. doi: 10.1128/jvi.00431-18. PubMed PMID: 29769338.
- 757 14. Hou J-N, Chen T-H, Chiang Y-H, Peng J-Y, Yang T-H, Cheng C-C, et al. PERK  
758 Signal-Modulated Protein Translation Promotes the Survivability of Dengue 2 Virus-Infected  
759 Mosquito Cells and Extends Viral Replication. *Viruses*. 2017;9(9):262. PubMed PMID:  
760 doi:10.3390/v9090262.



- 761 15. Black TL, Barber GN, Katze MG. Degradation of the interferon-induced 68,000-M(r)  
762 protein kinase by poliovirus requires RNA. *Journal of Virology*. 1993;67(2):791-800. PubMed  
763 PMID: 7678306.
- 764 16. Borghese F, Sorgeloos F, Cesaro T, Michiels T. The Leader Protein of Theiler's Virus  
765 Prevents the Activation of PKR. *Journal of virology*. 2019;93(19):e01010-19. doi:  
766 10.1128/JVI.01010-19. PubMed PMID: 31292248.
- 767 17. Dzananovic E, McKenna SA, Patel TR. Viral proteins targeting host protein kinase R  
768 to evade an innate immune response: a mini review. *Biotechnology and Genetic Engineering*  
769 *Reviews*. 2018;34(1):33-59. doi: 10.1080/02648725.2018.1467151.
- 770 18. García MA, Meurs EF, Esteban M. The dsRNA protein kinase PKR: Virus and cell  
771 control. *Biochimie*. 2007;89(6):799-811. doi: <https://doi.org/10.1016/j.biochi.2007.03.001>.
- 772 19. Goodman DE, Pretto CD, Krepostman TA, Carnahan KE, Spindler KR. Enhanced  
773 Replication of Mouse Adenovirus Type 1 following Virus-Induced Degradation of Protein  
774 Kinase R (PKR). *mBio*. 2019;10(2):e00668-19. doi: 10.1128/mBio.00668-19.
- 775 20. Li C, Zhu Z, Du X, Cao W, Yang F, Zhang X, et al. Foot-and-mouth disease virus  
776 induces lysosomal degradation of host protein kinase PKR by 3C proteinase to facilitate virus  
777 replication. *Virology*. 2017;509:222-31. doi: <https://doi.org/10.1016/j.virol.2017.06.023>.
- 778 21. Park C, Peng C, Brennan G, Rothenburg S. Species-specific inhibition of antiviral  
779 protein kinase R by capripoxviruses and vaccinia virus. *Annals of the New York Academy of*  
780 *Sciences*. 2019;1438(1):18-29. doi: 10.1111/nyas.14000.
- 781 22. Tallóczy Z, Jiang W, Virgin HW, Leib DA, Scheuner D, Kaufman RJ, et al. Regulation  
782 of starvation- and virus-induced autophagy by the eIF2 $\alpha$  kinase signaling pathway. *Proceedings*  
783 *of the National Academy of Sciences*. 2002;99(1):190-5. doi: 10.1073/pnas.012485299.

- 784 23. Perot BP, Ingersoll MA, Albert ML. The impact of macroautophagy on CD8(+) T-cell-  
785 mediated antiviral immunity. *Immunol Rev.* 2013;255(1):40-56. Epub 2013/08/21. doi:  
786 10.1111/imr.12096. PubMed PMID: 23947346.
- 787 24. Tey S-K, Khanna R. Autophagy mediates transporter associated with antigen  
788 processing-independent presentation of viral epitopes through MHC class I pathway. *Blood.*  
789 2012;120(5):994-1004. doi: 10.1182/blood-2012-01-402404.
- 790 25. Calfon M, Zeng H, Urano F, Till JH, Hubbard SR, Harding HP, et al. IRE1 couples  
791 endoplasmic reticulum load to secretory capacity by processing the XBP-1 mRNA. *Nature.*  
792 2002;415(6867):92-6. doi:  
793 [http://www.nature.com/nature/journal/v415/n6867/supinfo/415092a\\_S1.html](http://www.nature.com/nature/journal/v415/n6867/supinfo/415092a_S1.html).
- 794 26. Iwakoshi NN, Pypaert M, Glimcher LH. The transcription factor XBP-1 is essential for  
795 the development and survival of dendritic cells. *The Journal of experimental medicine.*  
796 2007;204(10):2267-75. Epub 2007/09/17. doi: 10.1084/jem.20070525. PubMed PMID:  
797 17875675.
- 798 27. Osorio F, Tavernier SJ, Hoffmann E, Saeys Y, Martens L, Veters J, et al. The unfolded-  
799 protein-response sensor IRE-1[alpha] regulates the function of CD8[alpha]+ dendritic cells.  
800 *Nat Immunol.* 2014;15(3):248-57. doi: 10.1038/ni.2808  
801 <http://www.nature.com/ni/journal/v15/n3/abs/ni.2808.html#supplementary-information>.
- 802 28. Kamimura D, Bevan MJ. Endoplasmic Reticulum Stress Regulator XBP-1 Contributes  
803 to Effector CD8<sup>+</sup> T Cell Differentiation during Acute Infection. *The Journal of*  
804 *Immunology.* 2008;181(8):5433-41. doi: 10.4049/jimmunol.181.8.5433.
- 805 29. Palam LR, Baird TD, Wek RC. Phosphorylation of eIF2 Facilitates Ribosomal Bypass  
806 of an Inhibitory Upstream ORF to Enhance CHOP Translation. *Journal of Biological*  
807 *Chemistry.* 2011;286(13):10939-49. doi: 10.1074/jbc.M110.216093.

- 808 30. Chen Y-J, Tan BC-M, Cheng Y-Y, Chen J-S, Lee S-C. Differential regulation of CHOP  
809 translation by phosphorylated eIF4E under stress conditions. *Nucleic Acids Research*.  
810 2009;38(3):764-77. doi: 10.1093/nar/gkp1034.
- 811 31. Li J-K, Liang J-J, Liao C-L, Lin Y-L. Autophagy is involved in the early step of  
812 Japanese encephalitis virus infection. *Microbes and Infection*. 2012;14(2):159-68. doi:  
813 <https://doi.org/10.1016/j.micinf.2011.09.001>.
- 814 32. Sharma M, Bhattacharyya S, Nain M, Kaur M, Sood V, Gupta V, et al. Japanese  
815 encephalitis virus replication is negatively regulated by autophagy and occurs on LC3-I- and  
816 EDEM1-containing membranes. *Autophagy*. 2014;10(9):1637-51. doi: 10.4161/auto.29455.
- 817 33. Gannagé M, Dormann D, Albrecht R, Dengjel J, Torossi T, Rämer PC, et al. Matrix  
818 Protein 2 of Influenza A Virus Blocks Autophagosome Fusion with Lysosomes. *Cell Host &*  
819 *Microbe*. 2009;6(4):367-80. doi: <https://doi.org/10.1016/j.chom.2009.09.005>.
- 820 34. Arakawa M, Morita E. Flavivirus Replication Organelle Biogenesis in the Endoplasmic  
821 Reticulum: Comparison with Other Single-Stranded Positive-Sense RNA Viruses.  
822 *International Journal of Molecular Sciences*. 2019;20(9):2336. PubMed PMID:  
823 doi:10.3390/ijms20092336.
- 824 35. Barrows NJ, Anglero-Rodriguez Y, Kim B, Jamison SF, Le Sommer C, McGee CE, et  
825 al. Dual roles for the ER membrane protein complex in flavivirus infection: viral entry and  
826 protein biogenesis. *Sci Rep*. 2019;9(1):9711-. doi: 10.1038/s41598-019-45910-9. PubMed  
827 PMID: 31273220.
- 828 36. Rothan HA, Kumar M. Role of Endoplasmic Reticulum-Associated Proteins in  
829 Flavivirus Replication and Assembly Complexes. *Pathogens*. 2019;8(3):148. PubMed PMID:  
830 doi:10.3390/pathogens8030148.

- 831 37. Junjhon J, Edwards TJ, Utaipat U, Bowman VD, Holdaway HA, Zhang W, et al.  
832 Influence of pr-M Cleavage on the Heterogeneity of Extracellular Dengue Virus Particles.  
833 Journal of Virology. 2010;84(16):8353-8. doi: 10.1128/jvi.00696-10.
- 834 38. Yu I-M, Zhang W, Holdaway HA, Li L, Kostyuchenko VA, Chipman PR, et al.  
835 Structure of the Immature Dengue Virus at Low pH Primes Proteolytic Maturation. Science.  
836 2008;319(5871):1834-7. doi: 10.1126/science.1153264.
- 837 39. Khromykh AA, Varnavski AN, Westaway EG. Encapsidation of the flavivirus kunjin  
838 replicon RNA by using a complementation system providing Kunjin virus structural proteins  
839 in trans. Journal of virology. 1998;72(7):5967-77. doi: 10.1128/JVI.72.7.5967-5977.1998.  
840 PubMed PMID: 9621059.
- 841 40. Kimura-Kuroda J, Yasui K. Topographical analysis of antigenic determinants on  
842 envelope glycoprotein V3 (E) of Japanese encephalitis virus, using monoclonal antibodies.  
843 Journal of virology. 1983;45(1):124-32. doi: 10.1128/JVI.45.1.124-132.1983. PubMed PMID:  
844 6185694.
- 845 41. Kumar P, Sulochana P, Nirmala G, Chandrashekar R, Haridattatreya M,  
846 Satchidanandam V. Impaired T Helper 1 Function of Nonstructural Protein 3-Specific T Cells  
847 in Japanese Patients with Encephalitis with Neurological Sequelae. The Journal of Infectious  
848 Diseases. 2004;189(5):880-91.
- 849 42. Turtle L, Bali T, Buxton G, Chib S, Chan S, Soni M, et al. Human T cell responses to  
850 Japanese encephalitis virus in health and disease. The Journal of Experimental Medicine.  
851 2016;213(7):1331-52. doi: 10.1084/jem.20151517.
- 852 43. Kumar P, Krishna VD, Sulochana P, Nirmala G, Haridattatreya M, Satchidanandam V.  
853 Cell-mediated immune responses in healthy children with a history of subclinical infection  
854 with Japanese encephalitis virus: analysis of CD4+ and CD8+ T cell target specificities by

- 855 intracellular delivery of viral proteins using the human immunodeficiency virus Tat protein  
856 transduction domain. *J Gen Virol.* 2004;85(2):471-82. doi: 10.1099/vir.0.19531-0.
- 857 44. Aleyas AG, George JA, Han YW, Rahman MM, Kim SJ, Han SB, et al. Functional  
858 Modulation of Dendritic Cells and Macrophages by Japanese Encephalitis Virus through  
859 MyD88 Adaptor Molecule-Dependent and -Independent Pathways. *The Journal of*  
860 *Immunology.* 2009;183(4):2462-74. doi: 10.4049/jimmunol.0801952.
- 861 45. García-Nicolás O, Lewandowska M, Ricklin ME, Summerfield A. Monocyte-Derived  
862 Dendritic Cells as Model to Evaluate Species Tropism of Mosquito-Borne Flaviviruses. *Front*  
863 *Cell Infect Microbiol.* 2019;9:5-. doi: 10.3389/fcimb.2019.00005. PubMed PMID: 30746342.
- 864 46. Wang P, Hu K, Luo S, Zhang M, Deng X, Li C, et al. DC-SIGN as an attachment factor  
865 mediates Japanese encephalitis virus infection of human dendritic cells via interaction with a  
866 single high-mannose residue of viral E glycoprotein. *Virology.* 2016;488:108-19. doi:  
867 <https://doi.org/10.1016/j.virol.2015.11.006>.
- 868 47. Uhl M, Kepp O, Jusforgues-Saklani H, Vicencio JM, Kroemer G, Albert ML.  
869 Autophagy within the antigen donor cell facilitates efficient antigen cross-priming of virus-  
870 specific CD8+ T cells. *Cell Death & Differentiation.* 2009;16(7):991-1005. doi:  
871 10.1038/cdd.2009.8.
- 872 48. Su H-L, Liao C-L, Lin Y-L. Japanese Encephalitis Virus Infection Initiates  
873 Endoplasmic Reticulum Stress and an Unfolded Protein Response. *Journal of Virology.*  
874 2002;76(9):4162-71. doi: 10.1128/jvi.76.9.4162-4171.2002.
- 875 49. Lee Y-Y, Cevallos RC, Jan E. An upstream open reading frame regulates translation of  
876 GADD34 during cellular stresses that induce eIF2alpha phosphorylation. *J Biol Chem.*  
877 2009;284(11):6661-73. Epub 2009/01/08. doi: 10.1074/jbc.M806735200. PubMed PMID:  
878 19131336.

- 879 50. Wang Q, Xin X, Wang T, Wan J, Ou Y, Yang Z, et al. Japanese Encephalitis Virus  
880 Induces Apoptosis and Encephalitis by Activating the PERK Pathway. *Journal of Virology*.  
881 2019;93(17):e00887-19. doi: 10.1128/jvi.00887-19. PubMed PMID: 31189710.
- 882 51. Kaiser WJ, Upton JW, Mocarski ES. Viral modulation of programmed necrosis.  
883 *Current Opinion in Virology*. 2013;3(3):296-306. doi:  
884 <https://doi.org/10.1016/j.coviro.2013.05.019>.
- 885 52. Tovilovic G, Ristic B, Milenkovic M, Stanojevic M, Trajkovic V. The role and  
886 therapeutic potential of autophagy modulation in controlling virus-induced cell death. *Med Res*  
887 *Rev*. 2014;34(4):744-67. Epub 2013/10/15. doi: 10.1002/med.21303. PubMed PMID:  
888 24123125.
- 889 53. Goodall Megan L, Fitzwalter Brent E, Zahedi S, Wu M, Rodriguez D, Mulcahy-Levy  
890 Jean M, et al. The Autophagy Machinery Controls Cell Death Switching between Apoptosis  
891 and Necroptosis. *Developmental Cell*. 2016;37(4):337-49. doi: 10.1016/j.devcel.2016.04.018.
- 892 54. Loi M, Ligeon L-A, Münz C. MHC Class I Internalization via Autophagy Proteins. In:  
893 Ktistakis N, Florey O, editors. *Autophagy: Methods and Protocols*. New York, NY: Springer  
894 New York; 2019. p. 455-77.
- 895 55. Junjhon J, Lausumpao M, Supasa S, Noisakran S, Songjaeng A, Saraithong P, et al.  
896 Differential Modulation of prM Cleavage, Extracellular Particle Distribution, and Virus  
897 Infectivity by Conserved Residues at Nonfurin Consensus Positions of the Dengue Virus pr-M  
898 Junction. *Journal of Virology*. 2008;82(21):10776-91. doi: 10.1128/jvi.01180-08.
- 899 56. Sharma KK, Lim X-X, Tantirimudalige SN, Gupta A, Marzinek JK, Holdbrook D, et  
900 al. Infectivity of Dengue Virus Serotypes 1 and 2 Is Correlated with E-Protein Intrinsic  
901 Dynamics but Not to Envelope Conformations. *Structure*. 2019;27(4):618-30.e4. doi:  
902 <https://doi.org/10.1016/j.str.2018.12.006>.

- 903 57. Dowd KA, DeMaso CR, Pierson TC. Genotypic Differences in Dengue Virus  
904 Neutralization Are Explained by a Single Amino Acid Mutation That Modulates Virus  
905 Breathing. *mBio*. 2015;6(6):e01559-15. doi: 10.1128/mBio.01559-15.
- 906 58. Kuhn RJ, Zhang W, Rossmann MG, Pletnev SV, Corver J, Lenches E, et al. Structure  
907 of Dengue Virus: Implications for Flavivirus Organization, Maturation, and Fusion. *Cell*.  
908 2002;108(5):717-25. doi: [https://doi.org/10.1016/S0092-8674\(02\)00660-8](https://doi.org/10.1016/S0092-8674(02)00660-8).
- 909 59. Cao S, Li Y, Ye J, Yang X, Chen L, Liu X, et al. Japanese Encephalitis Virus wild  
910 strain infection suppresses dendritic cells maturation and function, and causes the expansion of  
911 regulatory T cells. *Virology Journal*. 2011;8(1):39. doi: 10.1186/1743-422X-8-39.
- 912 60. Li Y, Ye J, Yang X, Xu M, Chen L, Mei L, et al. Infection of mouse bone marrow-  
913 derived dendritic cells by live attenuated Japanese encephalitis virus induces cells maturation  
914 and triggers T cells activation. *Vaccine*. 2011;29(4):855-62. doi:  
915 <https://doi.org/10.1016/j.vaccine.2010.09.108>.
- 916 61. Hayashi-Nishino M, Fujita N, Noda T, Yamaguchi A, Yoshimori T, Yamamoto A. A  
917 subdomain of the endoplasmic reticulum forms a cradle for autophagosome formation. *Nature*  
918 *Cell Biology*. 2009;11(12):1433-7. doi: 10.1038/ncb1991.
- 919 62. Ylä-Anttila P, Vihinen H, Jokitalo E, Eskelinen E-L. 3D tomography reveals  
920 connections between the phagophore and endoplasmic reticulum. *Autophagy*. 2009;5(8):1180-  
921 5. doi: 10.4161/auto.5.8.10274.
- 922 63. Turtle L, Tatullo F, Bali T, Ravi V, Soni M, Chan S, et al. Cellular Immune Responses  
923 to Live Attenuated Japanese Encephalitis (JE) Vaccine SA14-14-2 in Adults in a JE/Dengue  
924 Co-Endemic Area. *PLOS Neglected Tropical Diseases*. 2017;11(1):e0005263. doi:  
925 10.1371/journal.pntd.0005263.
- 926 64. Gaiha GD, McKim KJ, Woods M, Pertel T, Rohrbach J, Barteneva N, et al.  
927 Dysfunctional HIV-specific CD8<sup>+</sup> T cell proliferation is associated with increased caspase-8

- 928 activity and mediated by necroptosis. *Immunity*. 2014;41(6):1001-12. Epub 2014/12/08. doi:  
929 10.1016/j.immuni.2014.12.011. PubMed PMID: 25526311.
- 930 65. Markoff L. Points to consider in the development of a surrogate for efficacy of novel  
931 Japanese encephalitis virus vaccines. *Vaccine*. 2000;18:26-32. doi:  
932 [https://doi.org/10.1016/S0264-410X\(00\)00038-4](https://doi.org/10.1016/S0264-410X(00)00038-4).
- 933 66. Mishra N, Boudewijns R, Schmid MA, Marques RE, Sharma S, Neyts J, et al. A  
934 Chimeric Japanese Encephalitis Vaccine Protects against Lethal Yellow Fever Virus Infection  
935 without Inducing Neutralizing Antibodies. *mBio*. 2020;11(2):e02494-19. doi:  
936 10.1128/mBio.02494-19.
- 937 67. Kozuch O, Mayer V. Pig kidney epithelial (PS) cells: a perfect tool for the study of  
938 flaviviruses and some other arboviruses. *Acta Virol*. 1975;19(6):498. Epub 1975/11/01.  
939 PubMed PMID: 1999.
- 940 68. Satchidanandam V, Kumar N, Jumani RS, Challu V, Elangovan S, Khan NA. The  
941 Glycosylated Rv1860 Protein of *Mycobacterium tuberculosis* Inhibits  
942 Dendritic Cell Mediated TH1 and TH17 Polarization of T Cells and Abrogates Protective  
943 Immunity Conferred by BCG. *PLoS Pathog*. 2014;10(6):e1004176. doi:  
944 10.1371/journal.ppat.1004176.
- 945 69. Uchil PD, Kumar AVA, Satchidanandam V. Nuclear Localization of Flavivirus RNA  
946 Synthesis in Infected Cells. *J Virol*. 2006;80(11):5451-64. doi: 10.1128/jvi.01982-05.
- 947 70. Wollweber L. E. Harlow and D. Lane (Editors), *Antibodies: A Laboratory Manual*. XIII  
948 + 726 S., 50 Abb., 62 Tab. Cold Spring Harbor 1988. Cold Spring Harbor Laboratory. \$50.00.  
949 ISBN: 0-87969-314-2. *Journal of Basic Microbiology*. 1990;30(3):164-. doi:  
950 10.1002/jobm.3620300304.
- 951 71. Hanekom WA, Hughes J, Mavinkurve M, Mendillo M, Watkins M, Gamielien H, et  
952 al. Novel application of a whole blood intracellular cytokine detection assay to quantitate



953 specific T-cell frequency in field studies. *Journal of Immunological Methods*. 2004;291(1–  
954 2):185-95. doi: 10.1016/j.jim.2004.06.010.

955 72. Nylander S, Kalies I, Brefeldin A, but not monensin, completely blocks CD69  
956 expression on mouse lymphocytes: - efficacy of inhibitors of protein secretion in protocols for  
957 intracellular cytokine staining by flow cytometry. *Journal of Immunological Methods*.  
958 1999;224(1):69-76. doi: 10.1016/s0022-1759(99)00010-1.

959 73. O'Neil-Andersen NJ, Lawrence DA. Differential Modulation of Surface and  
960 Intracellular Protein Expression by T Cells after Stimulation in the Presence of Monensin or  
961 Brefeldin A. *Clinical and Diagnostic Laboratory Immunology*. 2002;9(2):243-50. doi:  
962 10.1128/cdli.9.2.243-250.2001. PubMed PMID: PMC119934.

963 74. Roederer M, Nozzi JL, Nason MC. SPICE: Exploration and analysis of post-cytometric  
964 complex multivariate datasets. *Cytometry A*. 2011;79(2):167–74.

965 75. Rieger AM, Nelson KL, Konowalchuk JD, Barreda DR. Modified annexin  
966 V/propidium iodide apoptosis assay for accurate assessment of cell death. *J Vis Exp*.  
967 2011;(50):2597. doi: 10.3791/2597. PubMed PMID: 21540825.

968

969 **FIGURE LEGENDS**

970 **Figure 1. Differential modulation of the PERK-eIF2 $\alpha$  pathway by WT and vaccine strains**  
971 **of JEV.** (A) Progressive loss of PERK in WT JEV- infected cells. N2A cells were infected  
972 with P20778 and SA14-14-2 at a multiplicity of 10 and lysate equivalent to  $2 \times 10^5$  cells  
973 electrophoresed on SDS-10 % PAGE and transferred onto nitrocellulose membrane were  
974 immunoblotted with antibodies specific to PERK and GAPDH. 10 mM DTT served as a  
975 positive control. DTT-3 h treatment of cells with 10 mM DTT. Both phosphorylated and non-  
976 phosphorylated forms of PERK detected by the antibody are indicated. (B) Sequential  
977 immunoblotting of virus infected cell lysates harvested at the time points indicated, with  
978 antibodies specific to p-eIF2 $\alpha$ , total eIF2 $\alpha$  and GAPDH. AMD- cells treated for 18 h with 5  
979  $\mu$ g/ml AMD. Immunoblotting of virus infected cell lysates harvested at the time points  
980 indicated with antibodies specific to (C) CHOP and GAPDH, (D) ATF4, CHOP and GAPDH  
981 and (E) p-IRE1 $\alpha$ , XBP-1 and GAPDH. DTT-3 h treatment of cells with 10 mM DTT; Tm-5 h  
982 treatment of cells with 5  $\mu$ g/ml tunicamycin. Numbers on the right indicate sizes in kilo Daltons  
983 (kDa), of proteins detected in each panel.

984 **Figure 2. JEV NS1' protein induces constitutive expression of CHOP.** PS cells transduced  
985 with lentiviruses stably expressing codon optimized GFP (PS-cop-GFP), JEV P20778 NS1  
986 protein (PS-P20-NS1) or JEV P20778 NS1' protein (PS-P20-NS1') were harvested at indicated  
987 time points and immunoblotted with antibodies to the proteins indicated on the left. JEV  
988 proteins NS1 and NS1' were detected using the mAb H5D12 and CB1A2, respectively  
989 generated in this study. Longer exposure did not reveal CHOP expression in NS1-expressing  
990 cells. Numbers on the right indicate sizes in kDa, of proteins detected in each panel.

991 **Figure 3. Differential modulation of autophagy by WT and vaccine strains of JEV.** Lysates  
992 of N2A cells infected with P20778 or SA14-14-2 at a multiplicity of 10 were electrophoresed

993 on SDS-10 % PAGE and transferred onto nitrocellulose membrane. Immunoblotting with  
994 antibodies specific to (A) LC3B, p62 and GAPDH, (B) LC3B, JEV NS1 and GAPDH after  
995 infected N2A cells were either left untreated or treated for 4 h with 100 nM bafilomycin A  
996 before being harvested at the indicated time points, (C) ATG5, ATG7 and GAPDH, (D)  
997 Caspase-3 and GAPDH and (E) pMLKL, tMLKL and GAPDH. UI-uninfected cell lysate;  
998 DTT-3 h treatment of cells with 10 mM DTT; Tm- treatment of cells for 5 h with 5 µg/ml  
999 tunicamycin; 24h SS- cells maintained for 24 h in serum free medium; AMD- cells treated for  
1000 18 h with 5 µg/ml AMD. Numbers on the right indicate sizes in kDa, of proteins detected in  
1001 each panel.

1002 **Figure 4. ER chaperone levels are increased in SA14-14-2 infected cells.** Lysates of PS (A)  
1003 and N2A (B) cells infected with P20778 or SA14-14-2 at a multiplicity of 10 and harvested at  
1004 indicated time points were immunoblotted using antibodies specific to BiP, calnexin,  
1005 calreticulin and GAPDH as indicated. N2A- uninfected N2A cell lysate; DTT-3 h treatment of  
1006 cells with 10 mM DTT; Tm- treatment of cells for 5 h with 5 µg/ml tunicamycin. Numbers on  
1007 the right indicate sizes in kDa, of proteins detected in each panel.

1008 **Figure 5. Folding kinetics of JEV E protein.** PS cells infected with JEV P20778 (A) or SA14-  
1009 14-2 (B) for 18 h were metabolically labeled for 5 min with <sup>35</sup>S-labeled methionine and cysteine  
1010 followed by treatment with 10 mM DTT for 5 min to reduce cysteine sulphhydryl groups on  
1011 proteins. DTT was rapidly and extensively washed out and cells were reincubated in complete  
1012 warm medium for the indicated times. Cell monolayers were treated with 20 mM NEM on ice  
1013 for 10 min and lysates prepared without DTT were electrophoresed on SDS-7.5 % PAGE. PS  
1014 cells infected with JEV P20778 (C) or SA14-14-2 (D) for 18 h were metabolically labeled for  
1015 5 min followed by replacement of medium with warm MEM containing 20 mM each of  
1016 cysteine and methionine. Cell monolayers were treated with 100 mM DTT for 5 min at  
1017 indicated time-points of chase, washed, alkylated with 20 mM NEM on ice for 10 min and

1018 lysates were electrophoresed on SDS-7.5 % PAGE. H<sub>2</sub>O<sub>2</sub> was used at 100 μM for 5 min. The  
1019 R1, Ri and R2 reduced along with oxidized form Ox of E are denoted by arrows. Numbers  
1020 below the lanes provide the proportion of label in each form of E as denoted.

1021 **Figure 6. Efficient furin cleavage of SA14-14-2 prM protein.** (A) Extracellular virus  
1022 particles of P20778 and SA14-14-2 were ultracentrifuged on a 30 and 70 % discontinuous  
1023 sucrose gradient as described in STAR Methods. Fractions from the interface of 30 and 70 %  
1024 sucrose (lanes 1 to 4) and from the 70 % sucrose (lanes 5 and 6) were electrophored on SDS-  
1025 12.5 % PAGE and immunoblotted with antibodies specific to the envelope (CE3, top panel) or  
1026 prM (1C8, lower panel) proteins. The envelope, prM and cleaved pr proteins are indicated on  
1027 the left with their sizes in kDa on the right. (B) Cell lysates of N2A left uninfected (U) or  
1028 infected with P20778 (P) and SA14-14-2 (S) immunoblotted with antibodies specific to the  
1029 envelope (CE3, top panel) or prM (1C8, lower panel).

1030 **Figure 7. Superior immune activation by SA14-14-2.** (A) Percentage of CD3<sup>+</sup>CD4<sup>+</sup> and  
1031 CD3<sup>+</sup>CD8<sup>+</sup> T cells secreting IFN-γ, TNF-α or MIP-1β in response to stimulation with capsid  
1032 (top panel), envelope (middle panel) and NS3 (lower panel) proteins of JEV P20778 compiled  
1033 for healthy JEV infected volunteers (HV; N=10), SA14-14-2 vaccinated individuals (VAC;  
1034 N=9) and recovered JEV patient (JEV; N=17) groups with median and IQR reported.  
1035 Polyfunctional CD3<sup>+</sup>CD4<sup>+</sup> and CD3<sup>+</sup>CD8<sup>+</sup> T cells secreting a combination of IFN-γ, TNF-α,  
1036 IL-2 and MIP-1β in response to capsid and envelope are also shown. Significance between  
1037 CD4<sup>+</sup> and CD8<sup>+</sup> T cells within any group was determined using Mann Whitney U test while  
1038 differences between CD4/CD8 T cells across the 3 groups were tested using Kruskal-Wallis H  
1039 test with Dunn's correction for multiple comparisons. (B) Enhanced cell death in SA14-14-2  
1040 infected antigen presenting cells. BMDC (left panel) and human THP-1 monocytes (right  
1041 panel) were left uninfected or infected at 1 m.o.i. with P20778 or SA14-14-2 for 24 h prior to  
1042 staining with Annexin V-FITC and propidium iodide (PI) as described in STAR Methods.

1043 Percentage positive cells are shown. N=4. Significant differences between groups were tested  
1044 using ANOVA with Bonferroni correction for multiple comparisons. (C) Secretion of  
1045 cytokines IL-12p40, TNF- $\alpha$  and IL-6 from BMDC infected with P20778 or SA14-14-2 for 12  
1046 h. NT-untreated; LPS- lipopolysaccharide from *E. coli* used at 0.1  $\mu\text{g/ml}$  for 8 h. N=4.  
1047 Significant difference between P20778 and SA14-14-2 strains of JEV was determined using  
1048 Mann Whitney U test. P values are interpreted as follows: \*,  $P \leq 0.05$ ; \*\*,  $P \leq 0.01$ ; \*\*\*,  $P \leq$   
1049 0.001; \*\*\*\*,  $P \leq 0.0001$ .

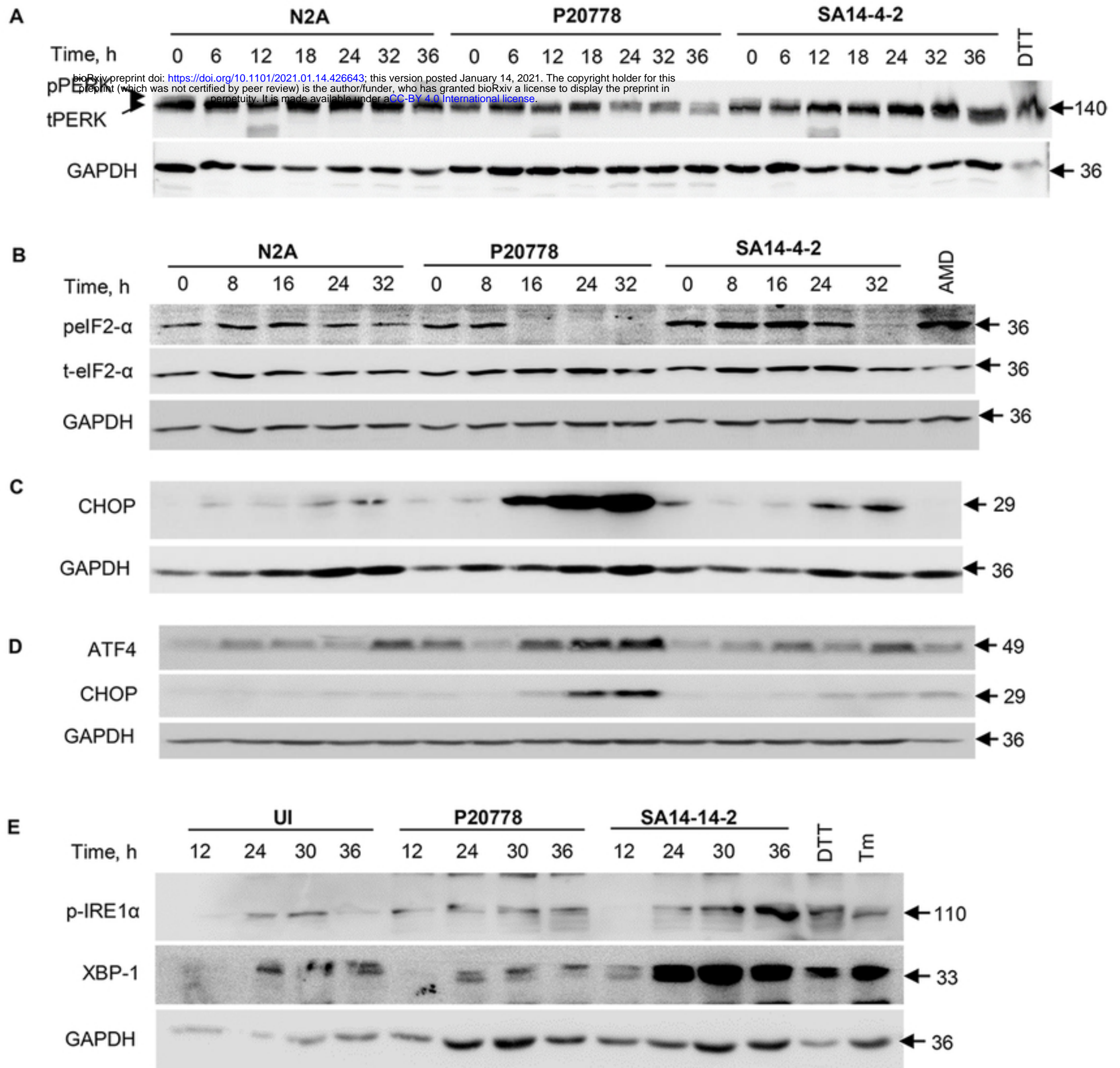


Fig1.tif



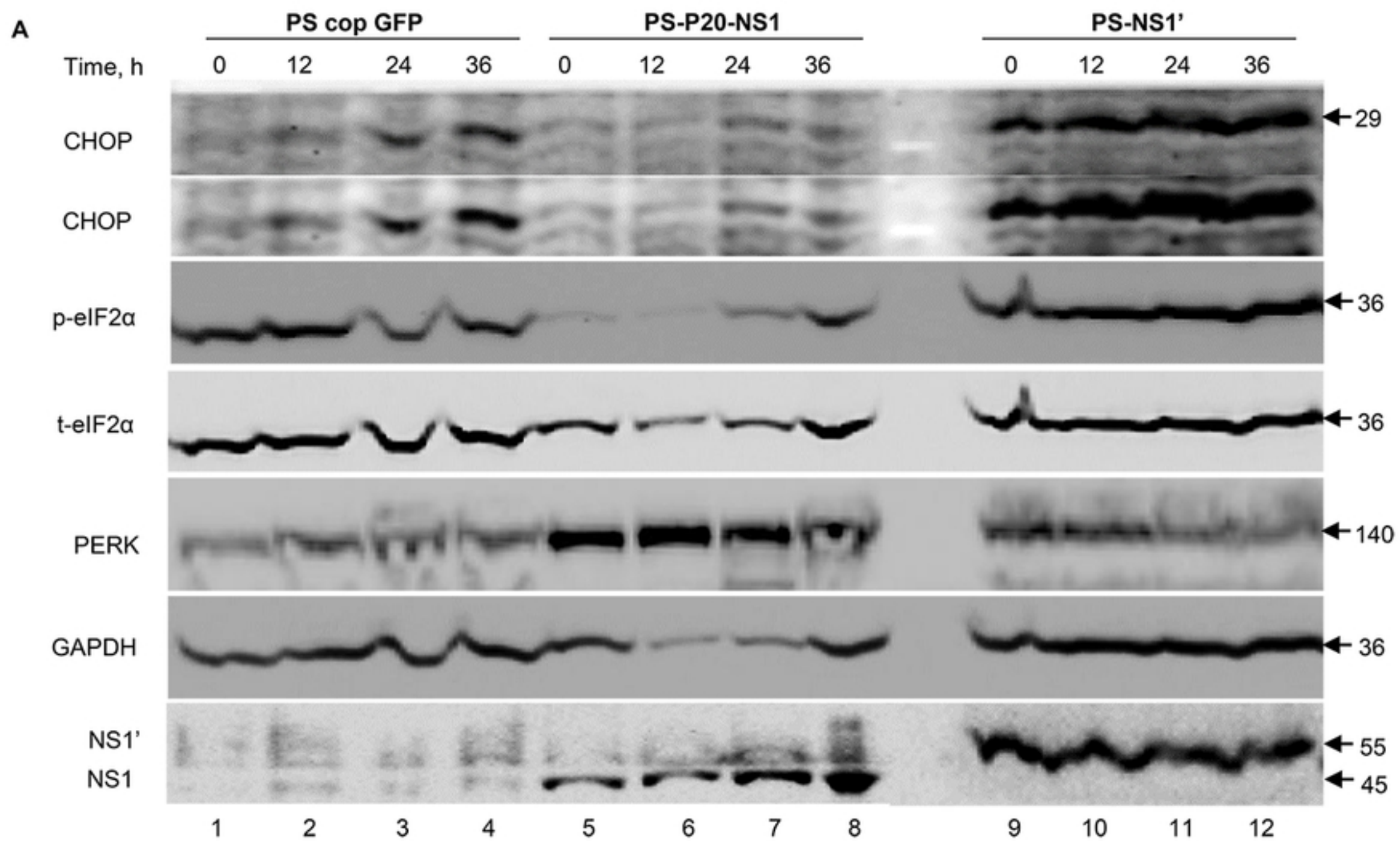


Fig2.tif

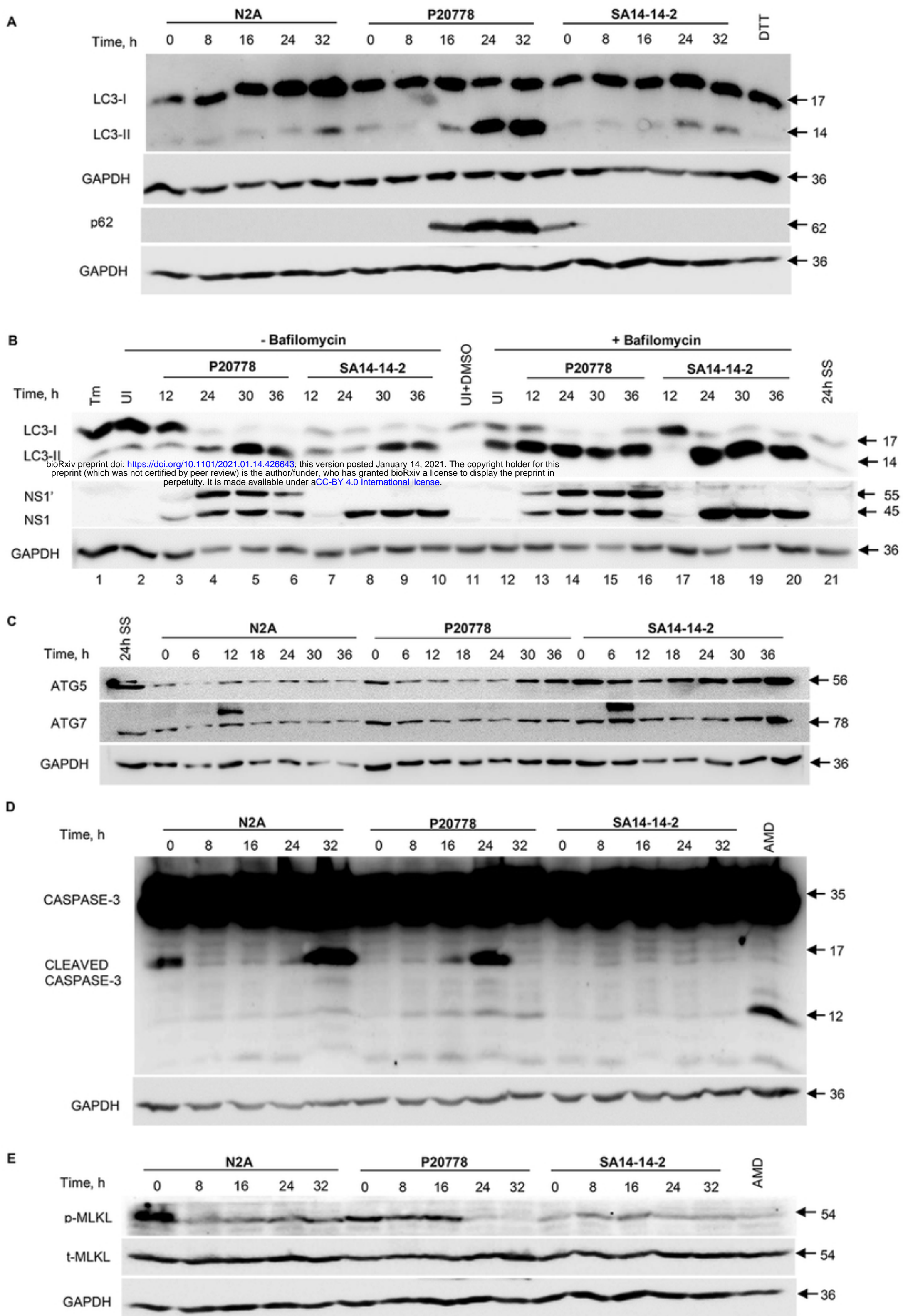


Fig3.tif



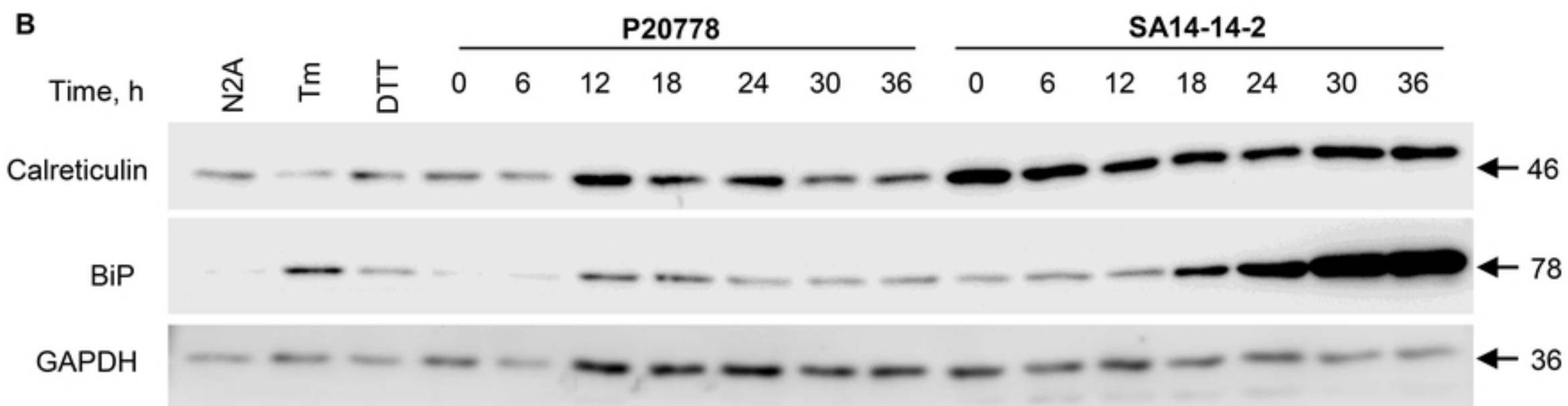
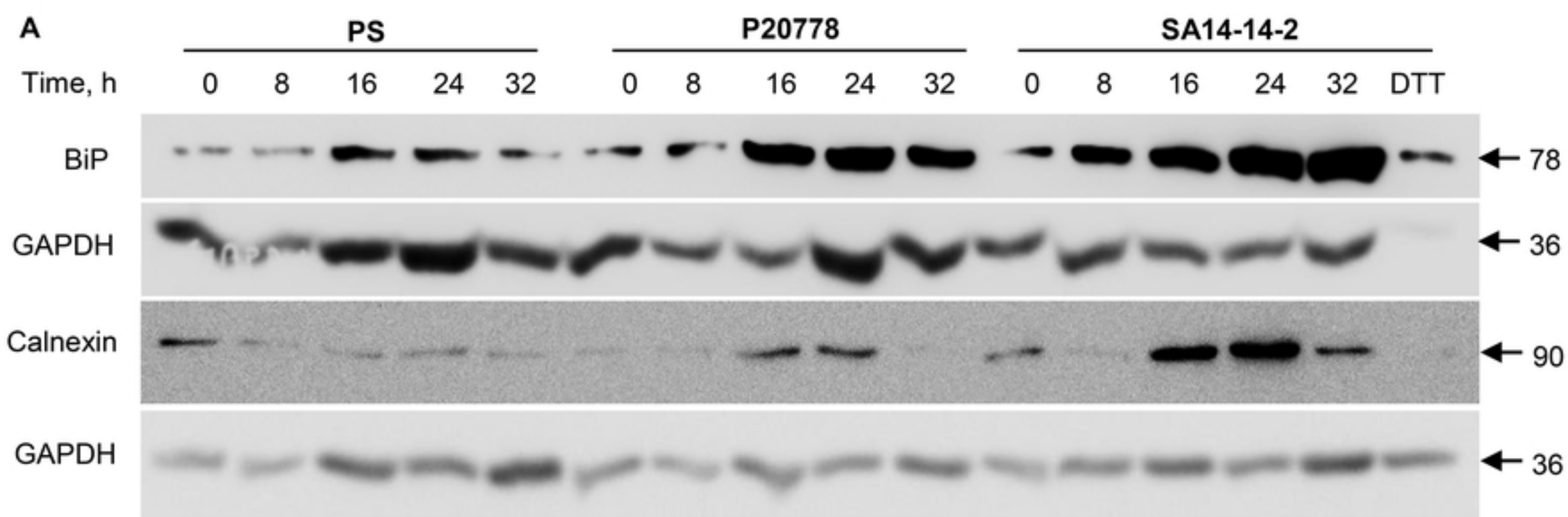


Fig4.tif

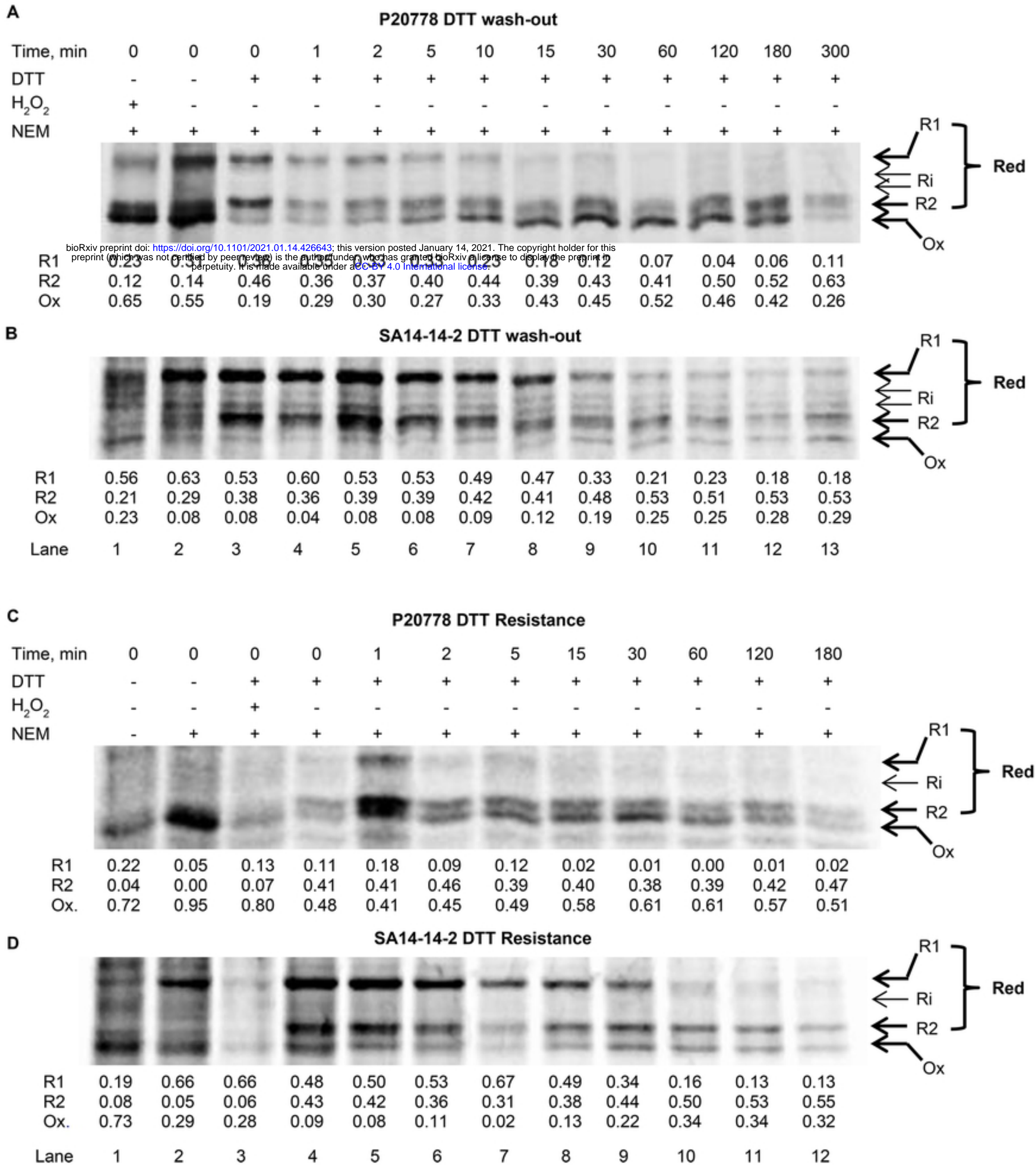


Fig5.tif

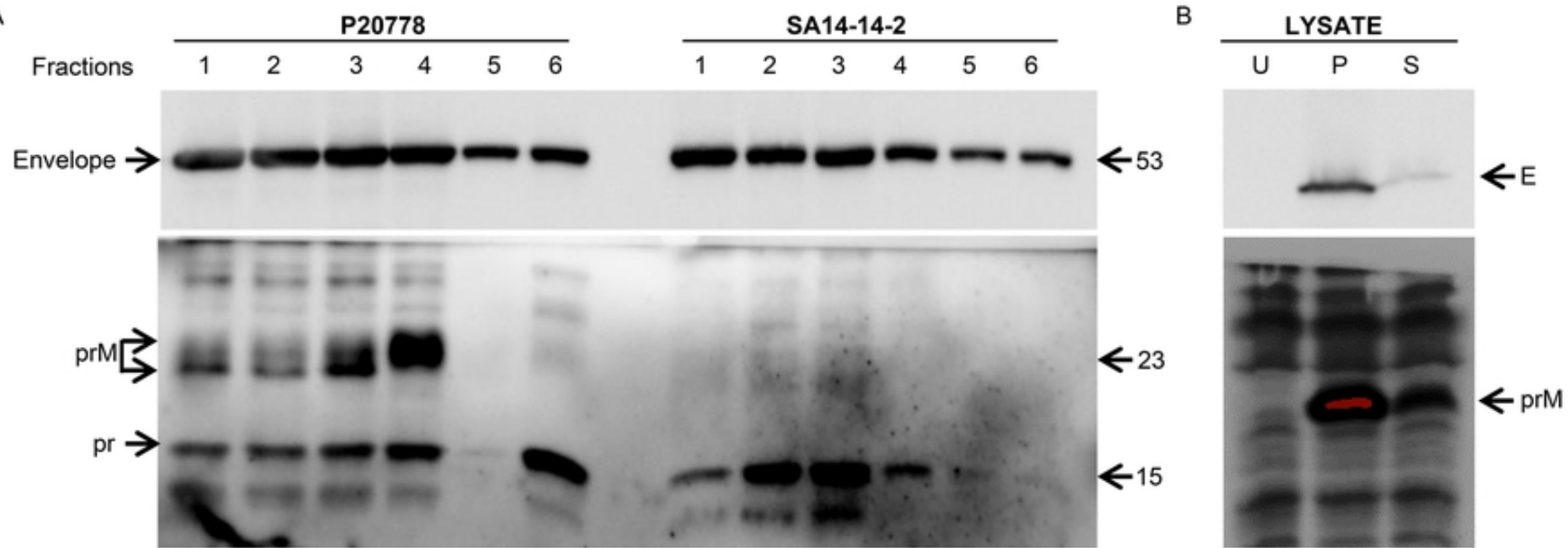


Fig6.tif

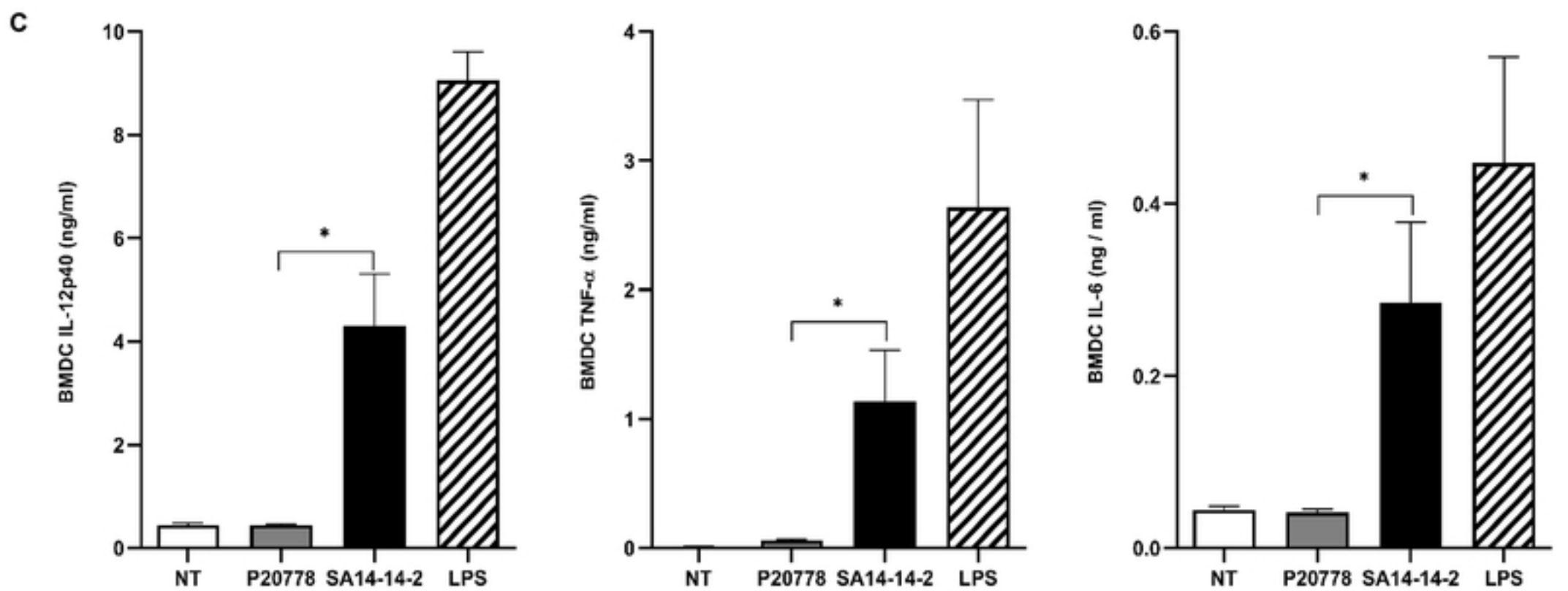
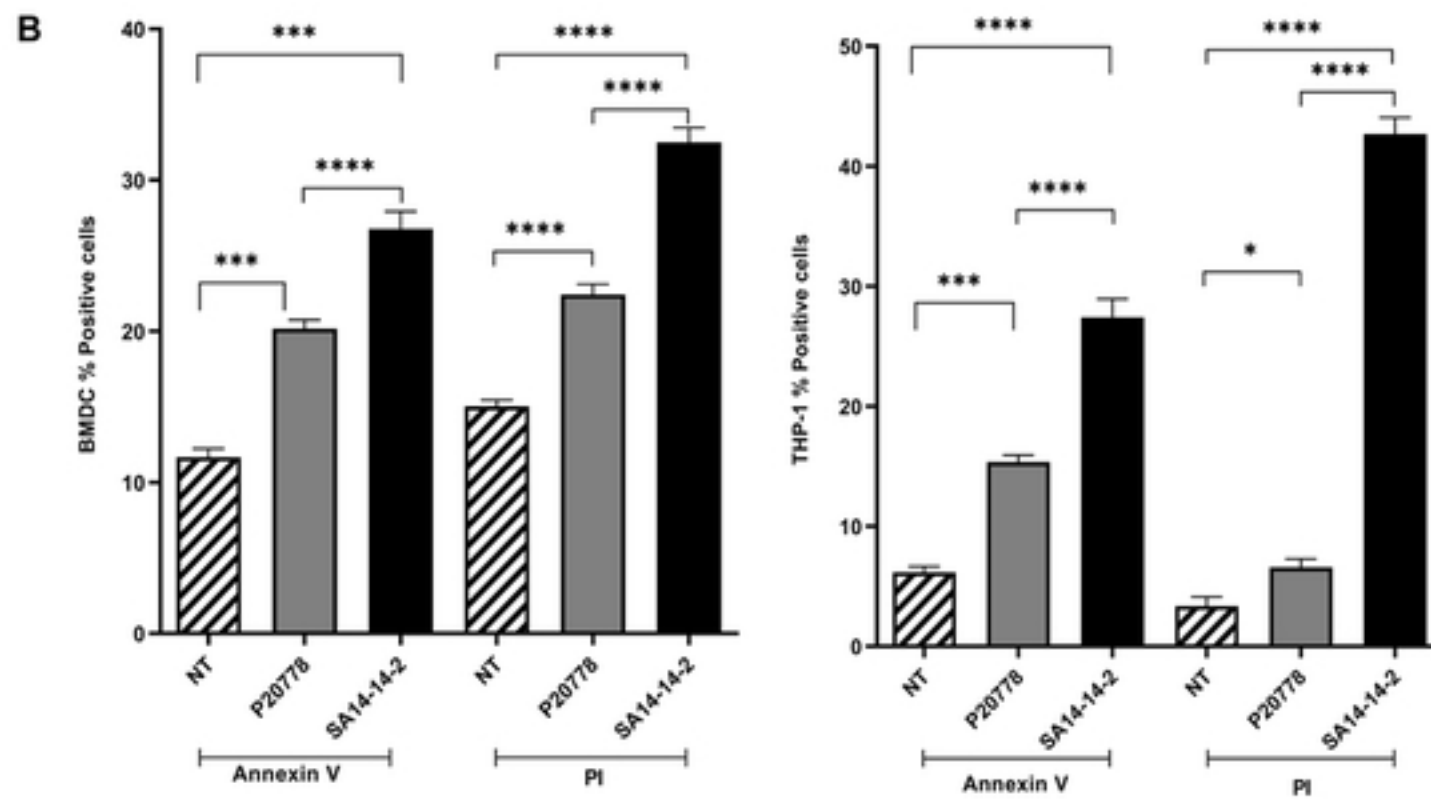
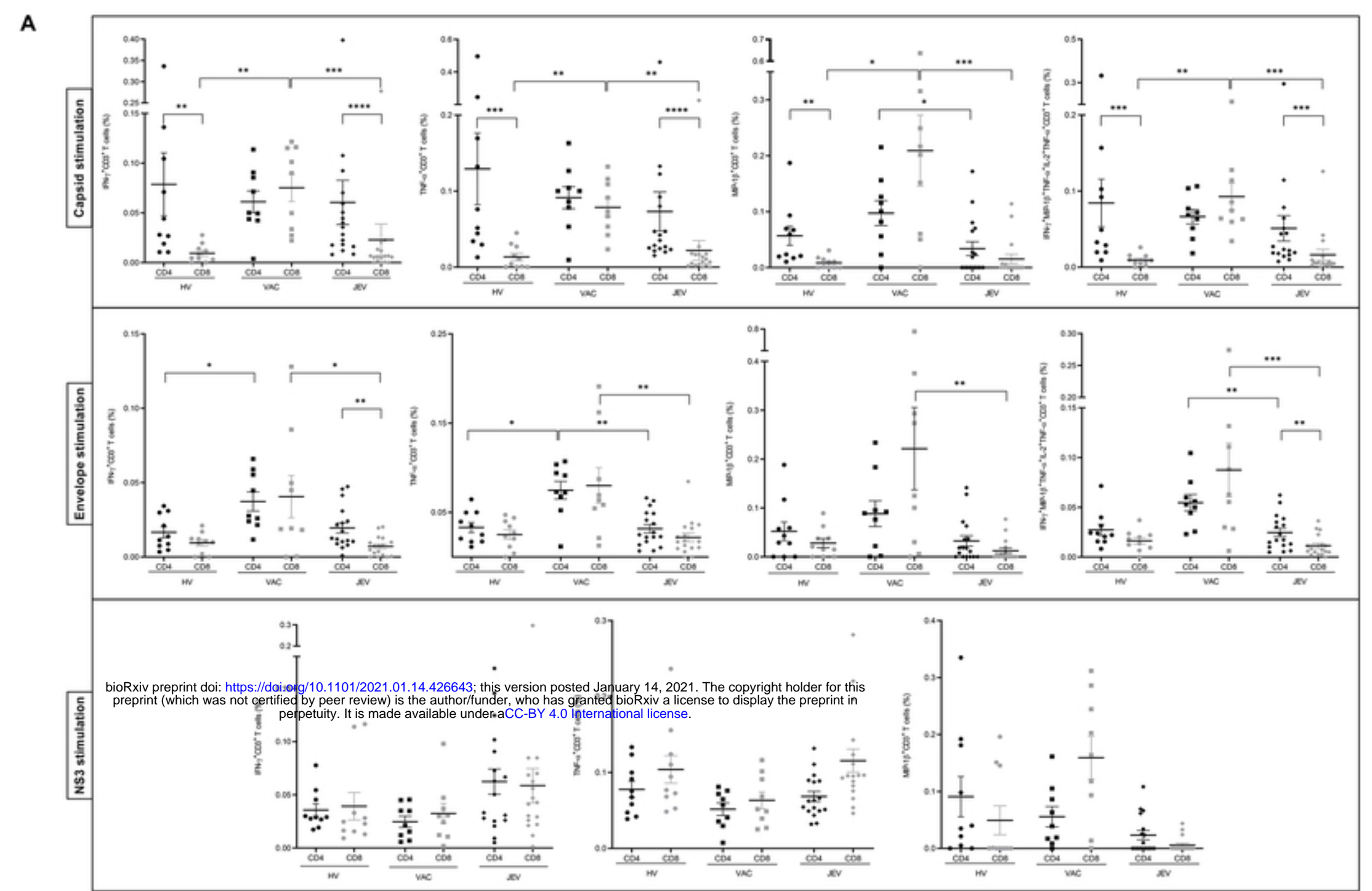


Fig7.tif